Environmental Analysis of GOES-R Proving Ground Convection-Initiation Forecasting Algorithms

JASON M. APKE

Atmospheric Sciences Department, University of Alabama in Huntsville, Huntsville, Alabama

DANIEL NIETFELD

NOAA/National Weather Service Weather Forecast Office Omaha/Valley, Valley, Nebraska

MARK R. ANDERSON

Department of Earth and Atmospheric Sciences, University of Nebraska—Lincoln, Lincoln, Nebraska

(Manuscript received 28 July 2014, in final form 11 November 2014)

ABSTRACT

Enhanced temporal and spatial resolution of the Geostationary Operational Environmental Satellite–R Series (GOES-R) will allow for the use of cloud-top-cooling-based convection-initiation (CI) forecasting algorithms. Two such algorithms have been created on the current generation of GOES: the University of Wisconsin cloud-top-cooling algorithm (UWCTC) and the University of Alabama in Huntsville's satellite convection analysis and tracking algorithm (SATCAST). Preliminary analyses of algorithm products have led to speculation over preconvective environmental influences on algorithm performance. An objective validation approach is developed to separate algorithm products into positive and false indications. Seventeen preconvective environmental variables are examined for the positive and false indications to improve algorithm output. The total dataset consists of two time periods in the late convective season of 2012 and the early convective season of 2013. Data are examined for environmental relationships using principal component analysis (PCA) and quadratic discriminant analysis (QDA). Data fusion by QDA is tested for SATCAST and UWCTC on five separate case-study days to determine whether application of environmental variables improves satellite-based CI forecasting. PCA and significance testing revealed that positive indications favored environments with greater vertically integrated instability (CAPE), less stability (CIN), and more low-level convergence. QDA improved both algorithms on all five case studies using significantly different variables. This study provides an examination of environmental influences on the performance of GOES-R Proving Ground CI forecasting algorithms and shows that integration of QDA in the cloud-top-cooling-based algorithms using environmental variables will ultimately generate a more skillful product.

1. Introduction

Nowcasting convection initiation (CI) with geostationary satellite data is an established and skillful technique and will continue to improve with the launch of new instrumentation (Mecikalski and Bedka 2006; Sieglaff et al. 2011). The use of cloud-top-cooling (CTC) brightness-temperature changes to forecast CI was explored by Roberts and Rutledge (2003), who found, through comparisons of Geostationary Operational Environmental Satellite (GOES) imagery and Weather Surveillance Radar-1988 Doppler (WSR-88D), that the first 35-dBZ echo occurred approximately 30 min after large cooling rates were observed at the cloud tops of subfreezing (>0°C) quasi-stationary cloud pixels. As an immature cumulus builds vertically, the temperature observed at the cloud top decreases long before the first radar echo is observed. Roberts and Rutledge (2003) also observed that CTC can discriminate between storms with weak precipitation (<35 dBZ) and strong precipitation (>35 dBZ).

The demonstrated value of CTC for nowcasting CI led to the development of two GOES infrared (IR)-based CI forecasting algorithms. The University

Corresponding author address: Jason Apke, 320 Sparkman Dr., Huntsville, AL 35805.
E-mail: jason.apke@gmail.com

DOI: 10.1175/JAMC-D-14-0190.1

© 2015 American Meteorological Society

of Wisconsin–Madison cloud-top-cooling algorithm (UWCTC) uses a computationally inexpensive boxed averaging method to track cloud objects with complex logic to filter out horizontal-motion-based cooling (Sieglaff et al. 2011). The UWCTC products are forecast indications with units of measured vertical cooling [K $(15\,\mathrm{min})^{-1}$] using IR-only satellite trends. The UWCTC data are obtained from the University of Wisconsin Space Science and Engineering Center (SSEC 2013).

The University of Alabama in Huntsville satellite convection analysis and tracking algorithm (SATCAST) uses mesoscale atmospheric-motion vectors (Bedka and Mecikalski 2005) to track cloud objects of interest and to monitor changes in several spectral trends (Mecikalski and Bedka 2006; Walker et al. 2012). The changes in important spectral trends, which Mecikalski and Bedka (2006) called "interest fields," are input into a logistic regression equation to determine the strength of signal (SoS), or the probability that the cloud object will generate reflectivity $\geq 35\,\mathrm{dB}Z$ within the next hour. More recent versions of SATCAST (version 2.3, after April 2013) are beginning to incorporate preconvective environmental variables in the logistic regression equation for SoS (J. Mecikalski 2013, personal communication). The output of SATCAST is a grid of identified cloud objects with associated SoS values. The SATCAST data are obtained from the University of Alabama in Huntsville (UAH 2013).

Previous studies have done basic validations to test the skill of CI products (Mecikalski et al. 2008; Hartung et al. 2013), but only a few have speculated on the impact of the preconvective environment on CTC-based predictions of CI (Mecikalski et al. 2008; Sieglaff et al. 2011; Walker et al. 2012). Validations range from radar-based CI detection (Mecikalski and Bedka 2006; Mecikalski et al. 2008; Walker et al. 2012) to occurrence of lightning near CTC indications (Sieglaff et al. 2011). Mecikalski et al. (2008) and Walker et al. (2012) also noted a modest false-alarm ratio even after using optimized interest fields. Sieglaff et al. (2011) and Walker et al. (2012) both discuss the possibility that preconvective environments may lower observed skill values in the output satellite-based CI forecasts. Variables such as convective inhibition (CIN; Walker et al. 2012) or high storm motion (SM; Sieglaff et al. 2011) can change both the probability that convection will occur in an area and the ability of a satellite algorithm to correctly diagnose changes in brightness temperature.

The goal of this work is to consider the influence of the preconvective environment on algorithm performance. This study is designed to answer three questions: Do preconvective environments have an impact on satellite-based CI forecasting algorithms? Can preconvective environmental variables be applied to new satellite products through a data-fusion process? Is forecast skill improved through the incorporation of preconvective environmental variables into the CTC algorithms? To answer these questions, an objective validation method similar to that of Sieglaff et al. (2013) is developed to examine large samples of both SATCAST and UWCTC products. Positive and false indications from both algorithms are examined with respect to preconvective environments derived from the analyses of numerical weather prediction (NWP) models by using principal component analysis (PCA) and tests for statistically significant differences. Environmental variables identified to hinder satellite-based CI forecasting are examined for their potential in a data-fusion process. Data fusion is tested using a quadratic discriminant analysis (QDA) approach on select case studies during the 2013 convective season. It is the goal of this work to explore the utility of data fusion and whether it will ultimately create a more skillful forecasting product.

2. Method

Several CTC and satellite interest-field-based studies that were focused on the U.S. central plains have been performed (Roberts and Rutledge 2003; Mecikalski and Bedka 2006; Sieglaff et al. 2011; Walker et al. 2012). This study uses a similar region over the Great Plains (Fig. 1) to examine satellite-based CI forecasts. The area was chosen because of the radar coverage and the availability of in situ measurements through surface observations and radiosondes. For the environmental analysis, data from 20 July to 17 August 2012 (July study period) and from 17 April to 17 May 2013 (April study period) are used.

A large-scale mosaic radar dataset is needed to validate satellite-based convective algorithms. The National Mosaic and Multi-Sensor Quantitative Precipitation Estimation (NMQ) system radar dataset offers multiradar, multisensor coverage over the study region (Zhang and Qi 2010; Zhang et al. 2011). NMQ data are obtained from the National Severe Storms Laboratory (NSSL) in Norman, Oklahoma (NSSL 2013). In addition, an NWP model is needed to resolve a full three-dimensional picture of the environment containing the observed CI indications. The Rapid Refresh model (RAP) is an hourly-updating model with 50 vertical levels and a Lambert conformal ~13-km-resolution grid covering North America. The standard-pressure-level data that are produced and archived span from 1000 to 100 hPa, with a vertical resolution of 25 hPa. RAP data are obtained from the National Climatic Data Center in Asheville, North Carolina (NCDC 2013).

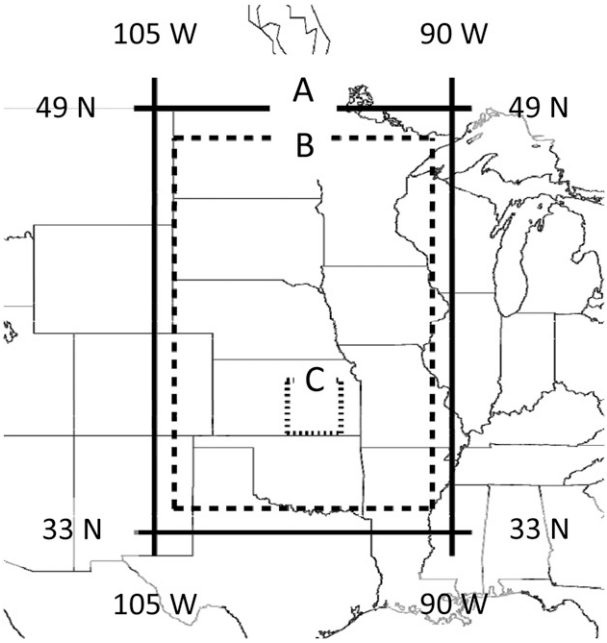

FIG. 1. Total area of study (solid outline labeled with A), parallax and track-corrected area of study (dashed outline, ranging from 91° to 104°W and from 34° to 48°N, labeled with B), and validation domain for CI truth clusters (dotted outline labeled with C).

a. *Defining convection initiation*

Validation first requires a definition for convection. A radar-based definition appropriately characterizes CI over the Great Plains and has been used in past studies (Roberts and Rutledge 2003; Mecikalski and Bedka 2006; Walker et al. 2012). For this study, CI is defined as the first occurrence of a radar return of 35 dBZ. Since our goal is to determine points of CI at any height, NMQ composite data are used. One advantage to using NMQ data is that the quality control procedures remove reflectivity issues that complicate identifying CI, such as bright banding, which helps to ensure that identified echoes are convective in nature (Zhang et al. 2011). The composite dataset requires radar-return segmentation and tracking for objective validation.

The "w2segmotionll" algorithm, which is part of the Warning Decision Support System–Integrated Information (WDSS-II) suite of algorithms, is utilized for this study. WDSS-II was developed by the NSSL and the Cooperative Institute for Mesoscale Meteorological Studies at the University of Oklahoma (Lakshmanan et al. 2007). The w2segmotionll algorithm clusters radar data on the basis of a combined k-means and enhanced-watershed technique (Lakshmanan and Smith 2009). The enhanced-watershed technique (Lakshmanan et al. 2009) is used on the quantized hierarchy of clusters in k-quanta space (Lakshmanan et al. 2003) to grow segmented clusters to a set minimum scale threshold. Clusters are then grown on these discrete increments from their maxima until a minimum scale threshold (saliency) is reached or surpassed. The segmentation method has the advantage of not being dependent on a threshold value only (e.g., ≥35 dBZ). The end result is an efficient cluster segmentation that allows for storm identification on a grid (Lakshmanan and Smith 2009).

To identify and track thunderstorms, the "Thunderstorm Observations by Radar" tracking algorithm (ThOR) was developed by the University of Nebraska (Houston et al. 2015). ThOR uses clusters identified in the w2segmotionll algorithm and storm-motion estimates to develop thunderstorm tracks. Tracking is achieved by considering all possible tracks within an acceptable error radius from a first-guess location. Extrapolated cluster positions are based on a combination of North American Regional Reanalysis (NARR) storm motion and observed storm motion (Houston et al. 2015; Lock and Houston 2014). Early in the track evolution (≤10 min), only NARR storm motion is used. Later in the track evolution (≥30 min), only observed motion is used. ThOR uses a weighted average between NARR storm motion and observed cluster motion to generate first-guess locations between 10 and 30 min. When a track is built, ThOR can use previously known locations to improve the guess as to where a cell is moving. Adaptive first-guess locations are advantageous relative to a storm-motion-only-based approach, in particular when tracking objects that are not constrained to the 0–6-km mean wind (e.g., supercells). Pixel clusters are tracked until they drop below a specific spatial threshold or move outside regions of interest. All possible tracks for a given cluster are considered, and ThOR assigns the track containing the smallest mean error (the average distance from the first-guess locations to the actual cluster locations). The first resolved cluster of a track is considered to be the CI cluster.

The combination of w2segmotionll and ThOR will objectively identify CI using NMQ data. The w2segmotionll algorithm requires a minimum spatial threshold to define a convective system. It also performs smoothing on a data grid to remove spurious peaks caused by data noise. The spatial and smoothing scales are determined using a subjective validation technique that is discussed in the appendix. The final product of the objective process (Fig. 2) is a two-dimensional grid of w2segmotionll-identified clusters at the same resolution as NMQ and is used for algorithm validation.

b. *Algorithm validation*

SATCAST, UWCTC, NMQ, and RAP are output on grids with ~1-km, ~4-km, ~1-km, and ~13-km gridpoint

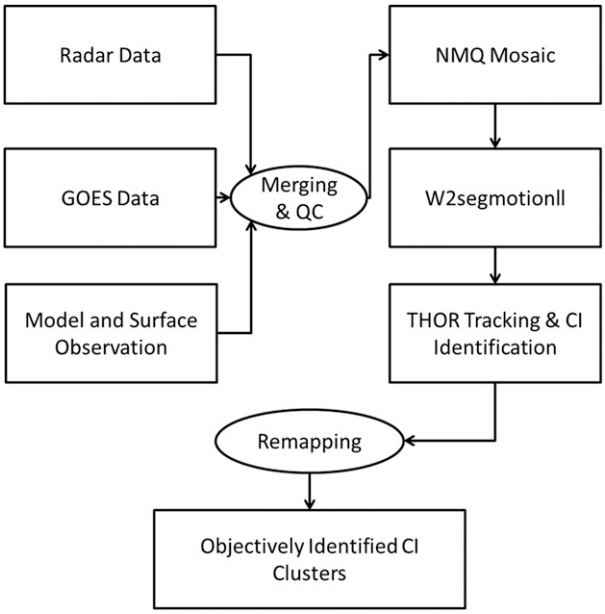

FIG. 2. Flowchart for defining CI.

spacings, respectively, and on different projections. All datasets are remapped to the SATCAST grid using a nearest-neighbor approach. Any discontinuities caused by grid-pixel centroids being located exactly between multiple pixels are resolved using the maximum value of the pixels in question. Discontinuities for the nearest-neighbor remapping approach only occurred on NMQ data, and therefore using the maximum value preserved any possible pixels ≥ 35 dBZ. SATCAST and UWCTC are produced on a grid of individual pixels; indications are considered as clusters, however. Clustering is done by grouping any neighboring pixels and considering them as a single indication. A UWCTC product is considered to be a CI indication if the cluster contains a value $< -4\,\mathrm{K}\,(15\,\mathrm{min})^{-1}$ (Roberts and Rutledge 2003; Sieglaff et al. 2011). SATCAST pixels are considered to be CI forecasts if any SoS value above 10% is detected (minimum output SoS value). As performed in Mecikalski and Bedka (2006) and Sieglaff et al. (2011), an indication that corresponds to the resolved CI cluster location within 1 h is considered to be a positive detection. If an indication occurs with no corresponding CI event, then that indication is considered to be false.

Since indications are witnessed up to 1 h before they are validated, the vertical development that created the indication is expected to advect out of its original location. Thus, CTC may be witnessed well upstream of the first 35-dBZ reflectivity cluster. To correct for storm motion, the validation process includes use of RAP-derived 0–6-km density-weighted storm-motion vectors to advect indication validation areas through time. When an indication is first detected, the storm-motion vector for that indication is used to advect the indication's validation area forward appropriately for each radar time step (every 5 min). It is acknowledged that the cloud-object depth may not extend through the 0–6-km layer, but the 0–6-km layer-mean wind is a sufficient representation of motion for cloud objects that are convective in nature (Mecikalski and Bedka 2006; Walker et al. 2012).

Although the nearest-neighbor approach does not change the values of the data, it does change the intended position of the forecast (with errors $< \sim 1$ km). Spatial correlation problems also exist when comparing satellite brightness-temperature values with reflectivity. A spatial displacement of satellite-based indications can also exist as a result of parallax. Parallax is resolved using a method similar to that in Sieglaff et al. (2011) in which indications are assumed to be at a height of 7 km. When correcting for parallax, ~0.5° is lost on all sides of the domain. To correctly identify CI points near the boundary of the domain using ThOR, another ~0.5° is used only to track objects and not for validation. The resulting domain ranges from 91° to 104°W and from 34° to 48°N (Fig. 1b). All other spatial correspondence issues are resolved through a subjective analysis. The subjective analysis is performed to validate indications as the algorithm would by comparing radar data with parallax-corrected satellite indications. The CI points are found by using the objective definition. Positive indications were found over a period of 4 h on 21 July 2012 across the entire domain. The process of identifying positive satellite indications involved identifying a cloud object as convective subjectively. The need for a subjective process here stems from the difficulty in backtracking satellite data at a 15-min temporal resolution. Objects identified objectively as convection by satellite would need to be appropriately backtracked to the correct preconvective cloud object, which would introduce several unwanted tracking errors at a low temporal resolution (Sieglaff et al. 2013). Subjective identification for the events involved avoids tracking errors, and, with the relatively isolated nature of the events used, subjective bias on identification of the correct cloud object is minimized. The positive centroids are advected and compared with the centroids of their respective CI detection (centroid distance) by using RAP-derived density-weighted 0–6-km storm motion. The centroid distance was compared with the average spatial radius (the average distance between an indication cluster centroid and cluster pixels) of both SATCAST and UWCTC indications. It was found that SATCAST pixels had a 2.96-km average spatial radius with CI centroid distances at 4.58 km. UWCTC indications on

average covered a larger area, with an average spatial radius of ~5.68 km and with CI centroid distances 5.86 km away. It is possible that this spatial error is caused by parallax issues or by problems with the process of remapping data. To compensate for the maximum possible spatial error, indications within approximately three pixels (~3 km) of a CI detection are considered to be positive forecasts.

A separate error that needs to be addressed in validation is the problem of multiple indications on a single storm changing the number of positive and false indications. If one system produces multiple indications, a system with several indications, either positive or false, would be favored in an environmental analysis over systems that may produce only a few indications. Data from GOES rapid scans would populate a larger sample size in study-period collections unless indications are tracked and coupled. ThOR is used to track indications from both UWCTC and SATCAST. An indication track is considered to be either one positive or one false indication. The track is positive if it contains an indication deemed to successfully forecast CI. Thus, from this point on, a positive or false indication refers to a group of tracked indications. The averages of environmental variables for the entire track are recorded for the single positive or false indication.

Tracking of satellite-based CI indications requires some changes from the radar-based tracking approach. Radar-based detections that are tracked are above the set spatial and reflectivity thresholds for deep convection and thus normally propagate with the mean 0–6-km wind. UWCTC indications are only given if substantial vertical cooling is identified, and they usually propagate in a manner that is similar to radar indications along the mean 0–6-km wind. SATCAST variables are produced on all clouds determined to be "preconvective" (Walker et al. 2012), and thus misidentified objects (edges of cirrus) may not be influenced by the lower-tropospheric wind at all. Although ThOR tracking with reasonable temporal scales (7–15 min) was able to handle this issue through track-weighted first-guess values, large temporal gaps on full disc scans created tracks deemed unreasonable upon closer examination. Thus, SATCAST tracks were not allowed to make temporal jumps ≥ 30 min, and new tracks were created after each full disc scan. SATCAST tracking with ThOR also had issues, with large numbers of candidate tracks being generated because of the large number of indications. Since ThOR considers all possible tracks for each indication, data-rich areas such as cumulus fields generated large numbers of candidate tracks that became unreasonable for computation. Excessive candidate tracks are mitigated by reducing the normal search radius of consideration and discarding tracks that would cause unreasonable mean error. By examining output candidate tracks, it was found that reducing the normal search radius to one-third of the radar-based default settings was a sufficient correction. Since the search radius around a first guess is a function of time, increasing with larger temporal data gaps (see Houston et al. 2015), the issue of too many candidate tracks will be mitigated with datasets that contain larger temporal resolution. In summary, SATCAST indications cannot currently be coupled across 30-min time gaps and the ThOR tracking radius is reduced to allow for reasonable computation by reducing the number of excessive candidate tracks. Both corrections with SATCAST tracking should be noted by the reader, but both corrections should not be necessary when this study is repeated on higher-temporal-resolution data with the launch of GOES-R.

c. *Environmental analysis*

The remapped RAP data are used with validated SATCAST and UWCTC indications to help to explain why some indications are positive while others are false. Since products are evaluated in clusters, environments can vary for different regions of SATCAST and UWCTC indications. Environmental variables for an indication are considered to be the average of the indication clusters' spatial and temporal domain. All grid points in the clusters along the track are averaged to give a representative preconvective environment of the indication. This study focuses on variables that would influence vertical growth of CI and its detection by satellite (Table 1).

All algorithms use brightness-temperature differences to derive areas of upward vertical motion (Mecikalski and Bedka 2006; Sieglaff et al. 2011; Mecikalski et al. 2013). When one is diagnosing areas that are prone to convective motion, parcel-theory-based convective variables are useful forecasting tools (Williams and Renno 1993). An environment that contains larger CAPE values is more conducive to faster transitions from immature cumulus to mature cumulonimbus (Mecikalski et al. 2013). Additional parcel-theory variables used include CIN, level of free convection (LFC), equilibrium level (EL), and lifted condensation level (LCL), which are dependent on the lifted parcel level (LPL). A most unstable approximation is used to account for both surface-based and elevated convection. The maximum pseudoequivalent potential temperature θ_e in the lowest 300 hPa is set as the LPL. Parcel-theory variables are supplemented by layer depths, including from the LCL to the LFC ($Z_{\mathrm{LFC\text{-}LCL}}$) and from the LFC to the EL ($Z_{\mathrm{EL\text{-}LFC}}$).

TABLE 1. List of variables used with respective abbreviations (abbr) and descriptions.

Variable	Abbr	Description
Convective available potential energy	CAPE	Total integrated positive buoyancy from the LFC to the EL
Convective condensation level	CCL	Level at which the surface mixing ratio meets the temperature profile
Convective inhibition	CIN	Total integrated negative buoyancy from the LPL to the LFC
Equilibrium level	EL	Level above LFC at which a lifted parcel becomes cooler than the surrounding environment
Lifted condensation level	LCL	Level at which a lifted parcel saturates
Level of free convection	LFC	Level at which an adiabatically lifted parcel becomes warmer than the surrounding environment
Lifted parcel level	LPL	Level of max θ_e in the lowest 300 hPa
LPL divergence	LPLD	$\nabla \cdot \mathbf{V}$ composite value calculated at the LPL
Lapse rates	LR	Change in temperature with respect to height calculated at several levels (0–3 km; 700–500 hPa)
Mean wind differential	MWD	Magnitude of the vector change in wind velocity (0–6 km)
Normalized CAPE	NCAPE	CAPE divided by the LFC − EL depth
Normalized CIN	NCIN	CIN divided by the LPL − LFC depth
Layer relative humidity	RH	Avg relative humidity calculated from the LCL to the LFC
Storm motion	SM	Averaged layer of mean wind from 0 to 6 km, assumed to be the characteristic storm motion
Convective environmental difference	$T_c - T_e$	Approximation of cumulus-field formation potential; the difference of the convective and environmental temperatures
EL − LFC	$Z_{\text{EL-LFC}}$	Distance in meters from the LFC to the EL
LFC − LCL	$Z_{\text{LFC-LCL}}$	Distance in meters from the LCL to the LFC

Positive and false indications are compared with the layers through which a convective parcel will have to traverse, including $Z_{\text{LFC-LCL}}$ and $Z_{\text{EL-LFC}}$. Large values of $Z_{\text{LFC-LCL}}$ are indicative of deep inversion layers that hinder both convective development and algorithmic cooling identification (Walker et al. 2012). Layer $Z_{\text{EL-LFC}}$ is examined to monitor the convective cooling depth throughout the unstable layer. Areas with larger $Z_{\text{EL-LFC}}$ have greater adiabatic temperature change throughout parcel excursion and are easier for brightness-temperature-differencing algorithms to resolve correctly. CAPE is also normalized throughout the depth of the unstable layer (NCAPE) and can parameterize a parcel's susceptibility to entrainment during ascent. Large NCAPE values suggest that the environment is conducive to more explosive development (less entrainment) with larger buoyant accelerations in a layer. Normalized CIN (NCIN) is also calculated. Lower NCIN values (more negative) are a characteristic of deeper stable layers, which, if a parcel is allowed to cool through a deeper layer, may be more prone to producing false identification (Walker et al. 2012). This study also examines the influence of 0–6-km mean wind differential (MWD; Weisman and Klemp 1984), lapse rates from the 0–3-km height (LOWLR) and 700–500-hPa pressure levels (MIDLR), mean relative humidity from the LCL to the LFC (RH), convective condensation level (CCL), convective temperature depression ($T_c - T_e$), divergence resolved at the lifted parcel level (LPLD; see Banacos and Schultz 2005), and density-weighted 0–6-km SM. Storm motion is included, as mentioned in both Sieglaff et al. (2011) and Walker et al. (2012), to reduce the likelihood that convection is incorrectly detected by satellite-based CI forecasting algorithms.

The temporal granularity of the RAP is an important limitation in convective-time-scale studies. Convection can occur on 0–1-h time scales, whereas the RAP products are received and updated on only an hourly basis. Thus, convective events that occur on subhour time scales change the environmental parameters in a way that cannot be detected by using RAP analysis. Since convection-contaminated environments cannot yet be resolved with sufficient temporal resolution by operational NWP models, areas near ongoing convection are removed from datasets used for statistical analysis. This study uses a 50-km-radius mask (~7850 km^2) around all w2segmotionll-resolved convective clusters to identify what are considered to be contaminated (and therefore unused) areas. The 50-km radius ensures that convective events cannot advect into areas that are being considered for preconvective environmental analysis

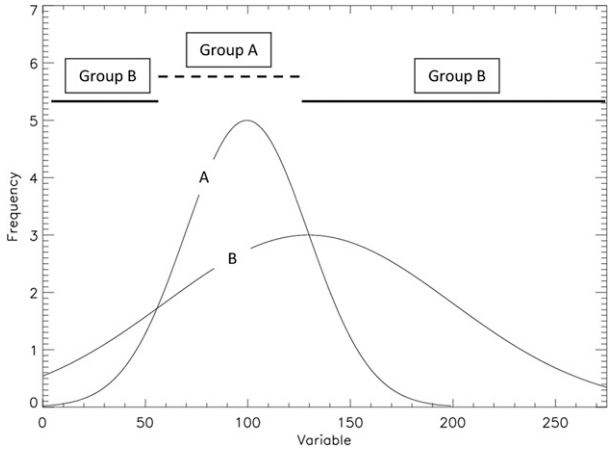

FIG. 3. Sample variable-distribution comparison performed by QDA. Two group distributions are presented: group A and group B. QDA will use these distributions to classify new data into groups on the basis of probability (area under the curve). For example, if these distributions were to be used to classify a new point with a variable value of 100, that variable would be assigned to group A given a higher probability. In this paper, this technique is performed on a multivariate basis.

on sub-RAP (<60 min) time scales. The 50-km-radius mask does not directly affect calculation of validation statistics because RAP variables are not required in determining algorithm performance.

d. Data fusion

The final step of this study is to take the environmental variable analysis of positive and false indications and use it on future products to improve satellite-only CI forecasting algorithms. Once the original CTC algorithms are validated and the environmental variables are found for each indication, two different statistical approaches are used. The first is PCA. PCA is a simple statistical way to reduce the dimensionality of data (Hotelling 1933). The PCA method was previously used to analyze the variation in several satellite-based interest fields in Mecikalski et al. (2008). The top two principal components are resolved and plotted with respect to positive and false indications.

The second statistical approach taken is in the form of Z statistics that are based on the Mann–Whitney (MW) test (Mann and Whitney 1947). The MW approach is not sensitive to nonnormality in datasets given that it is an examination of ranked data. Statistically significant differences are applied to a probability-based data-fusion method. Several data-fusion methods are available for use; for example, logistic regression is used for the current version of SATCAST (Mecikalski et al. 2015). Since the goal of this work is to identify and remove indications that are false in nature on the basis of environmental data, the method chosen is a QDA (Fisher 1936). Discrimination and classification are techniques designed to separate sets of observations into groups and to allocate new observations to those groups using the gathered statistical data (Johnson and Wichern 2007). QDA works by comparing the probability of an indication coming from a group to prior estimated probabilities that an indication is within a group (Fig. 3). Probability density functions that are based on environmental data are generated with statistical databases by using the objective validation. If there is no statistically significant difference in a particular environmental variable between positive and false groups of indications, the probability from the density functions for both groups will be approximately equal. Therefore, if a statistically significant difference is not found for an environmental variable, it is removed from QDA.

TABLE 2. Transformations done to normalize convective-variable distributions. These transformations are used in the statistical tests, and results are reported in the original forms. Variables that are not in this table were left untransformed.

Variable	Transformation
CAPE	$x^{1/2}$
NCAPE	$x^{1/6}$
CIN	$-1 \times (\lvert x \rvert)^{1/5}$
NCIN	$-1 \times (\lvert x \rvert)^{1/9}$
LPL	$x^{1/2}$
LFC	$x^{1/2}$
EL	$x^{1.5}$
CCL	$x^{1/2}$

QDA relies on the assumption of multivariate normality to determine probability density functions of positive and false indications. In the atmosphere, most data are not always normally distributed. Nonnormal distributions are resolved through variable transformation (Table 2). The MW approach is not sensitive to nonnormality in datasets given that it is an examination of ranked data (Mann and Whitney 1947).

In mathematical terms, the derivation for a QDA comes from the minimized expected-cost-of-misclassification function, which Johnson and Wichern (2007) show to be

$$\mathrm{ECM} = c(2\,|\,1)P(2\,|\,1)p_1 + c(1\,|\,2)P(1\,|\,2)p_2\,,$$

where p_1 and p_2 are prior probabilities of an indication being from group 1 or 2, $c(1\,|\,2)$ and $c(2\,|\,1)$ are costs of misclassification, and $P(2\,|\,1)$ and $P(1\,|\,2)$ are the probabilities of misclassification. Johnson and Wichern (2007) show that the function is minimized by allocation of observations to groups in the following way:

TABLE 3. Example confusion matrix. Columns represent QDA classification, and rows represent actual classification. The percentage of improvement is found with $j = 100\%[(a/e) - (c/f)]$.

		Predicted		
		False	Positive	Total
Actual	False	a	b	e
	Positive	c	d	f
	Total	g	h	i
Percentage of improvement:			j	

Observation $\mathbf{x}_o$ is allocated to group 1 if

$$\frac{P(\mathbf{x}_o)_1}{P(\mathbf{x}_o)_2} \geq \frac{c(1\,|\,2)p_2}{c(2\,|\,1)p_1}.$$

The left-hand side of the equation is the ratio of probability density functions that an indication lies within group 1 or 2 on the basis of $\mathbf{x}_o$ (the indications-corresponding matrix of m environmental variables). If the environmental data are a multivariate normal distribution, the probability density functions on the left-hand side of the equation are defined as

$$P(\mathbf{x}_o)_n = \frac{1}{(2\pi)^{m/2}|\boldsymbol{\Sigma}_n|^{1/2}} \exp\left[-\frac{1}{2}(\mathbf{x}_o - \boldsymbol{\mu}_n)'\boldsymbol{\Sigma}_n^{-1}(\mathbf{x}_o - \boldsymbol{\mu}_n)\right],$$

where $\boldsymbol{\Sigma}_n$ refers to the $m \times m$ population covariance matrix of group n and $\boldsymbol{\mu}_n$ is an $m \times 1$ matrix of the population average environmental variables for group n (Johnson and Wichern 2007; Wilks 2011). If it is assumed that positive and false indication environmental data have equal covariance matrices, the left-hand side of the equation simplifies to a comparison of covariance-weighted distances to prior probabilities (also known as a linear discriminant analysis). By assuming equal costs of misclassifications and equal prior probabilities, the discriminant function becomes a simple comparison of covariance-weighted distances (i.e., if environmental data of an indication are closer to the statistical database of environmental data for positive indications than to the one for false indications, that indication is classified as a positive indication). In this study, the assumption that the covariance matrices are equal is not made, and the resulting allocation function is as follows:

Observation $\mathbf{x}_o$ is allocated to group 1 if

$$-\frac{1}{2}x_o'(S_1^{-1} - S_2^{-1})x_o + (\bar{x}_1'S_1^{-1} - \bar{x}_2'S_2^{-1})x_o - k \geq \ln\left[\left(\frac{c(1\,|\,2)}{c(2\,|\,1)}\right)\left(\frac{p_2}{p_1}\right)\right],$$

where k is defined as

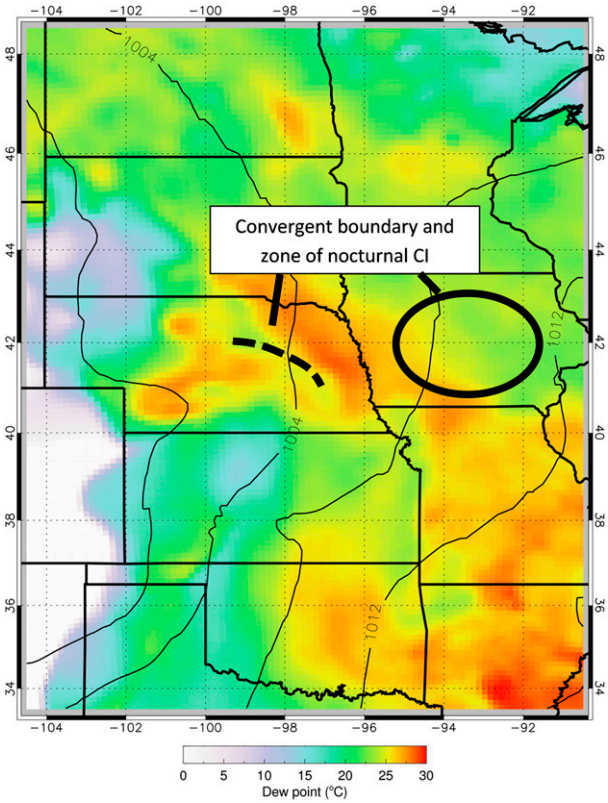

FIG. 4. RAP MSLP (contours; hPa) and surface dewpoint (shading; °C) at 0200 UTC 25 Jun 2013.

$$k = \frac{1}{2}\ln\left(\frac{|\mathbf{S}_1|}{|\mathbf{S}_2|}\right) + \frac{1}{2}(\bar{\mathbf{x}}_1'\mathbf{S}_1^{-1}\bar{\mathbf{x}}_1 - \bar{\mathbf{x}}_2'\mathbf{S}_2^{-1}\bar{\mathbf{x}}_2),$$

where $\mathbf{S}_n$ refers to the $m \times m$ sample covariance matrix of group n and $\bar{\mathbf{x}}_n$ is an $m \times 1$ matrix of the sample average environmental variables for group n (Johnson and Wichern 2007). If the observation does not satisfy the condition, it is assigned to group 2. The sample covariance matrix and sample mean matrix are derived from the data collected, and new data stored in $\mathbf{x}_o$ are used from different case studies. Costs of misclassification are assumed to be equal in this study. Costs can be adjusted by future users to weight the discriminant function toward assigning a specific group if necessary.

Prior probabilities are also not assumed to be equal. Current SoS values are probabilities of CI within the next hour calculated through multivariate logistic regression of satellite interest fields and environmental variables from a database that contains ~9000 subjectively validated indications (Mecikalski et al. 2015). Prior probabilities are used when discriminating SATCAST data, where p_1 is the probability that a detection will be false (1 − SoS) and p_2 is just SoS. Use of SoS values as prior probabilities allows us to weight the QDA on the basis

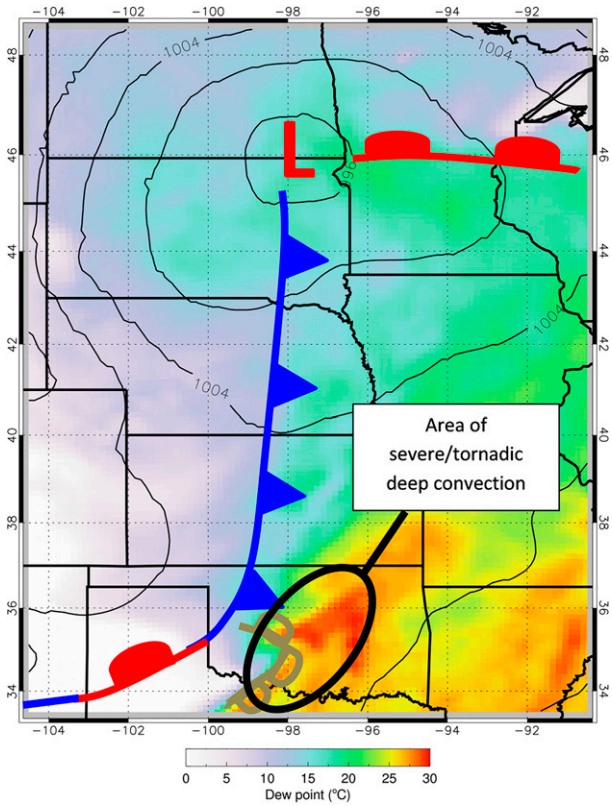

FIG. 5. As in Fig. 4, but at 1800 UTC 20 May 2013 and showing surface boundaries.

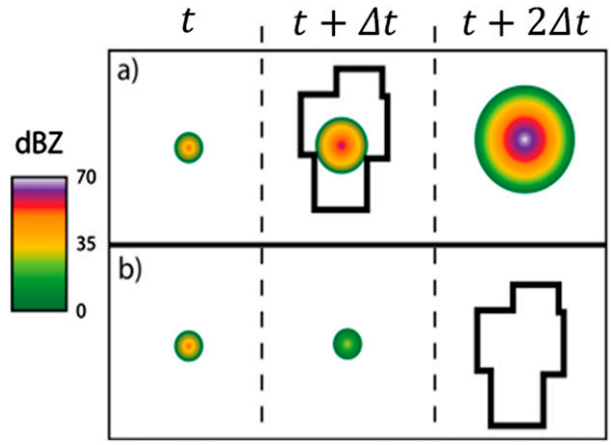

FIG. 6. Radar reflectivity (dBZ) at three time steps, where initiation occurs at time t. The black-outlined polygons represent CTC indications. (a) Example of a positive post-CI CTC indication, in which reflectivity values intensify after cooling. (b) Example of a false CTC detection occurring after CI, with no nearby ongoing convection.

of previous successful derivations of probability of CI for a given indication. The training dataset for calculation of the environmental covariance and mean matrices in QDA was created without considering SoS values, and therefore statistical differences found between indication groups are not affected. Use of SoS as prior probabilities will act to merge the two statistical approaches for incorporation of environmental variables and should not harm the end result of the QDA. If a variable is deemed not significantly different, however, a QDA can be further improved if the SoS value does not consider the environmental variable in question. Although the calculation of SoS is beyond the scope of this paper, future studies can use the statistically significant differences found in environmental variables of positive and false indications to improve new product output.

Since UWCTC is not produced in probability format, prior probabilities are estimated on the basis of the given CTC value. Here, p_2 is assumed to be 0.25 for weak UWCTC signals [$-10 < \mathrm{CTC} < -4\,\mathrm{K}\ (15\,\mathrm{min})^{-1}$], 0.5 for moderate signals [$-20 < \mathrm{CTC} < -10\,\mathrm{K}\ (15\,\mathrm{min})^{-1}$], and 0.75 for strong signals [$\mathrm{CTC} < -20\,\mathrm{K}\ (15\,\mathrm{min})^{-1}$] (Hartung et al. 2013). The assignment of these probabilities is acknowledged to be heuristic; because these products are evolving to probability-based systems (Cintineo et al. 2014), however, the assignment is meant to provide future users with examples on how to properly use the QDA database. Prior probabilities used here conform to prior understanding of CTC and CI (Sieglaff et al. 2011; Hartung et al. 2013), and can be adjusted by future users to account for observed indications with different parameterizations.

QDA performance is evaluated on separate case studies that have been collected and are not part of the original dataset. Evaluation is done using a dichotomous confusion matrix, which quantifies performance of a QDA by determining the matches between actual and classified groups (Table 3). QDA-resolved false variables are removed to create a filtered satellite-based forecasting product. In previous literature, it was common to evaluate algorithm skill using validation statistics such as POD, FAR, and CSI (see the appendix) for UWCTC and Brier scores for SATCAST. The confusion-matrix approach is used to determine whether overall skill scores (CSI and Brier score) have changed by using the relative difference between positive and false indications. The percentage of improvement (POI) is the relative number of false indications removed in comparison with the relative number of positive indications removed. Positive POI values suggest that more false indications than positive indications have been removed; thus, the resulting product will have improved skill scores. Five case-study days in 2013 are selected to examine the effectiveness of the QDA using the confusion-matrix approach.

e. *Case studies*

The case studies are chosen to provide a variety of synoptic situations to test the QDA filtering approach.

TABLE 4. UWCTC PCA eigenvectors with amount of variation explained by the principal component. The top five variables are shown in boldface font for each principal component.

	Jul 2012		Apr 2013	
	PC1	PC2	PC1	PC2
CAPE	−0.279	**−0.321**	0.225	**−0.383**
CIN	−0.287	0.068	−0.076	−0.151
LCL	−0.007	**0.464**	−0.205	0.273
LFC	**0.365**	−0.069	**0.285**	**0.296**
EL	−0.281	−0.181	0.146	**−0.367**
RH	−0.071	−0.211	**0.288**	−0.104
LPL	0.180	0.015	**0.302**	0.252
LPLD	0.069	−0.073	0.059	0.002
$T_c - T_e$	**0.376**	−0.131	0.254	0.164
CCL	0.143	**0.423**	−0.151	0.200
MIDLR	0.067	0.242	−0.084	−0.105
LOWLR	**−0.320**	0.312	**−0.395**	−0.064
MWD	0.137	−0.103	0.265	0.215
NCAPE	−0.163	**−0.296**	0.284	**−0.322**
NCIN	−0.070	0.042	−0.109	0.025
$Z_{\text{EL-LFC}}$	**−0.398**	−0.110	−0.014	**−0.459**
$Z_{\text{LFC-LCL}}$	**0.326**	**−0.303**	**0.372**	0.124
SM	0.045	−0.185	0.266	−0.024
Variation explained (%)	27.10	18.03	29.46	22.46

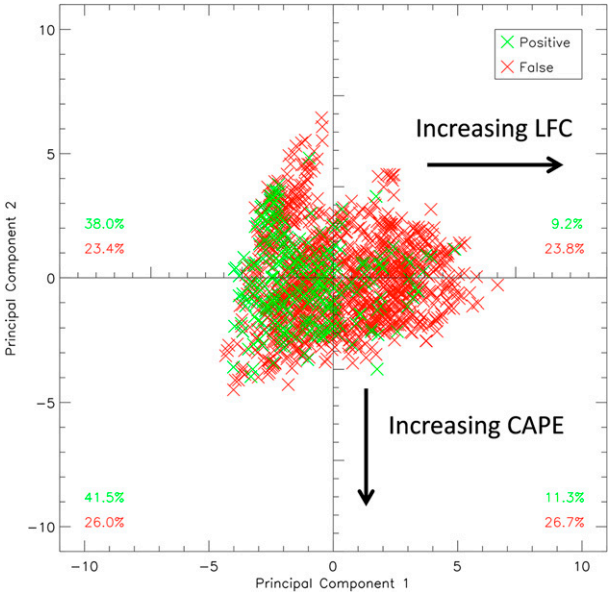

FIG. 7. Plot for the July UWCTC study period that shows the first (x axis) and second (y axis) principal components. Positive (false) UWCTC indications shown in green (red).

In chronological order, they are 1800 UTC 9 April–0300 UTC 10 April 2013, 1800 UTC 20 May–0000 UTC 21 May 2013, 1200 UTC 20 June–1200 UTC 22 June 2013 (two cases over 2 days), and 0000–1200 UTC 25 June 2013. The case studies range in scope from weak nocturnal convection (the 25 June 2013 case; Fig. 4) to high-impact severe-convection days (the 20 May 2013 case—the Moore, Oklahoma, tornado; Fig. 5). All case studies are used to evaluate QDA performance. An advantage of using case studies will be to understand how well probability-based data filtering will work in an operational setting.

3. Results

Objective validation determines positive and false groups within the July 2012 and April 2013 study periods. Objective validation also determined positive and false groups for selected case studies. For UWCTC environmental analysis there are 1211 (284) false (positive) indications during the July study period and 797 (391) false (positive) indications during the April study period. For SATCAST environmental analysis there are 357 496 (4209) false (positive) indications for the July study period and 282 965 (1160) false (positive) indications for the April study period. These numbers may seem daunting to prospective users, but the reader is reminded that these data are all indications that are at least 50 km away from ongoing convection. It is common for positive indications to be clustered along a boundary. If several positive indications occur near or along a boundary, the first indications will be collected in the dataset and all subsequent indications cannot be considered. Also, SATCAST indications are produced on all cloud types determined to be preconvective (Walker et al. 2012). SoS is only changed on the basis of witnessed interest fields. For the July study period, of the 357 496

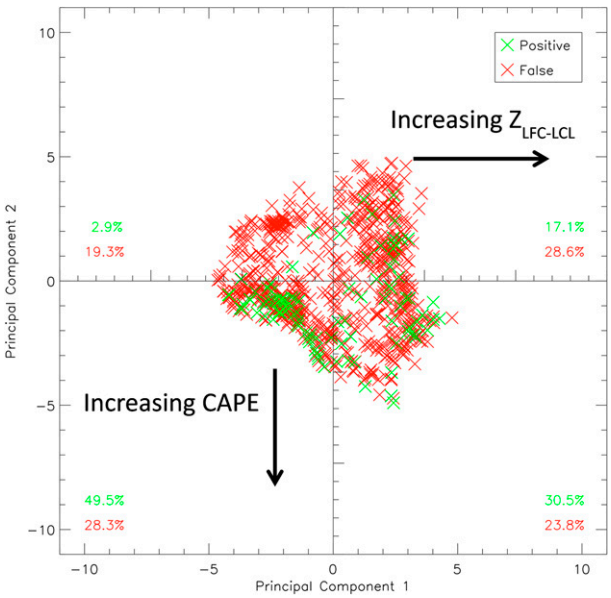

FIG. 8. As in Fig. 7, but for the April UWCTC study period.

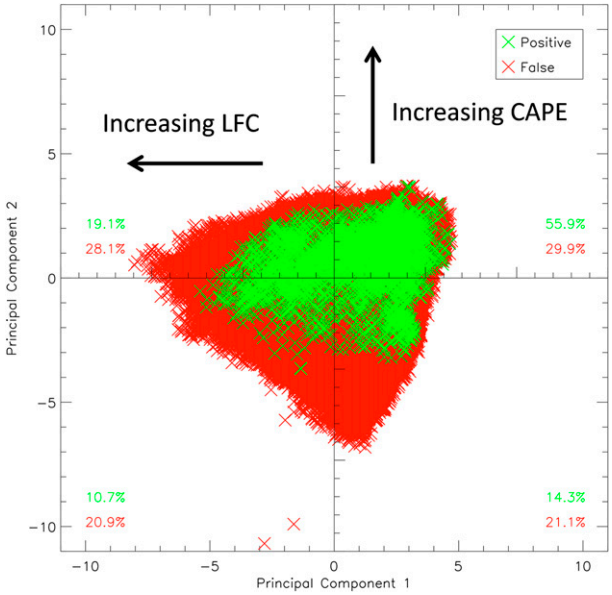

FIG. 9. As in Fig. 7, but for the July SATCAST study period.

TABLE 5. As in Table 4, but for SATCAST.

	Jul 2012		Apr 2013	
	PC1	PC2	PC1	PC2
CAPE	0.199	**0.310**	−0.053	**−0.458**
CIN	**0.297**	−0.067	−0.226	0.085
LCL	−0.146	0.225	0.117	**0.403**
LFC	**−0.417**	0.107	**0.441**	−0.033
EL	0.152	**0.448**	−0.097	**−0.428**
RH	0.132	−0.242	0.052	−0.207
LPL	−0.212	−0.013	**0.372**	0.049
LPLD	−0.015	−0.062	0.049	−0.017
$T_c - T_e$	**−0.397**	0.050	**0.397**	−0.038
CCL	−0.259	**0.367**	0.153	**0.314**
MIDLR	−0.229	0.259	0.114	−0.084
LOWLR	0.289	0.231	**−0.361**	0.260
MWD	−0.046	−0.236	0.162	−0.038
NCAPE	0.001	0.003	0.005	−0.018
NCIN	0.001	0.019	−0.001	0.005
$Z_{\text{EL-LFC}}$	**0.326**	**0.337**	−0.289	**−0.359**
$Z_{\text{LFC-LCL}}$	**−0.340**	−0.034	**0.367**	−0.259
SM	0.075	**−0.382**	0.126	−0.138
Variation explained (%)	25.28	15.37	24.11	16.76

false indications found, 187 355 indications are below 30% SoS (~50% of false indications). Approximately 85% of the 4209 positive indications have SoS values that are greater than 30%. For the April study period, of the 282 965 false indications, 254 025 contain an SoS value of less than 30% (~90% of false indications). Also, 457 positive indications, or 40% of positive indications, have an SoS value that is greater than 30%. The substantial improvement in SoS value for the false indications in the April SATCAST is due to the incorporation of convective variables into the SoS value calculation. SATCAST output from after April of 2013 now includes several convective variables in the logistic regression equation, including CAPE, CIN, LCL, LFC, CCL, and many others that will be discussed in upcoming publications (J. Mecikalski 2013, personal communication). There are still a large number of false indications with SoS values of greater than 30%, which suggests that QDA incorporation may be helpful.

A simple test of how well the validation works is to compare the skill scores found here with previous findings. Since the current UWCTC algorithm was extensively analyzed for skill in previous studies, this algorithm was chosen for subjective interpretation. The objective validation approach produced a 36.1% POD and 45.5% FAR for the UWCTC algorithm. The validation statistics for UWCTC presented here are less skillful than the statistics that are found in Sieglaff et al. (2011) and Hartung et al. (2013) (FAR values of ~40% and POD of ~50%). UWCTC presented a 45.2% POD and 27% FAR with subjective validation. Upon closer examination, many subjectively identified positive indications occurred after CI was detected on a complex. A post-CI CTC indication is a satellite-based indication that occurs on a convective complex after it has reached spatial and quantitative thresholds for reflectivity that were set to identify CI. Most post-CI CTC indications were indicators of a strengthening system in which reflectivity would increase after the forecast was made. Since subjective validation considers post-CI CTC

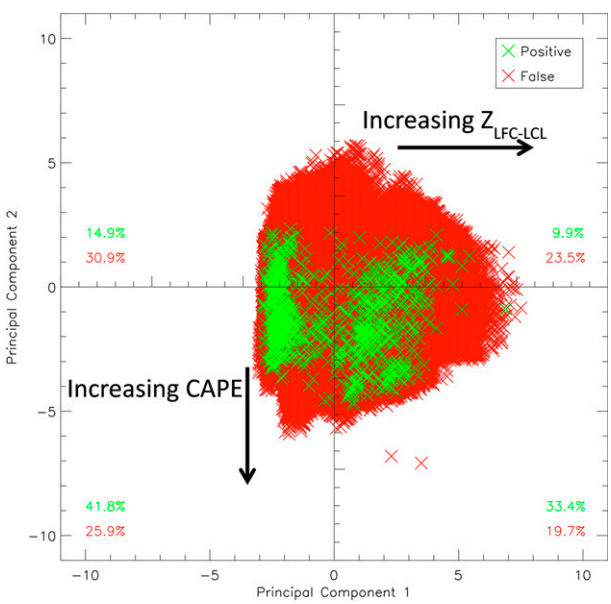

FIG. 10. As in Fig. 7, but for the April SATCAST study period.

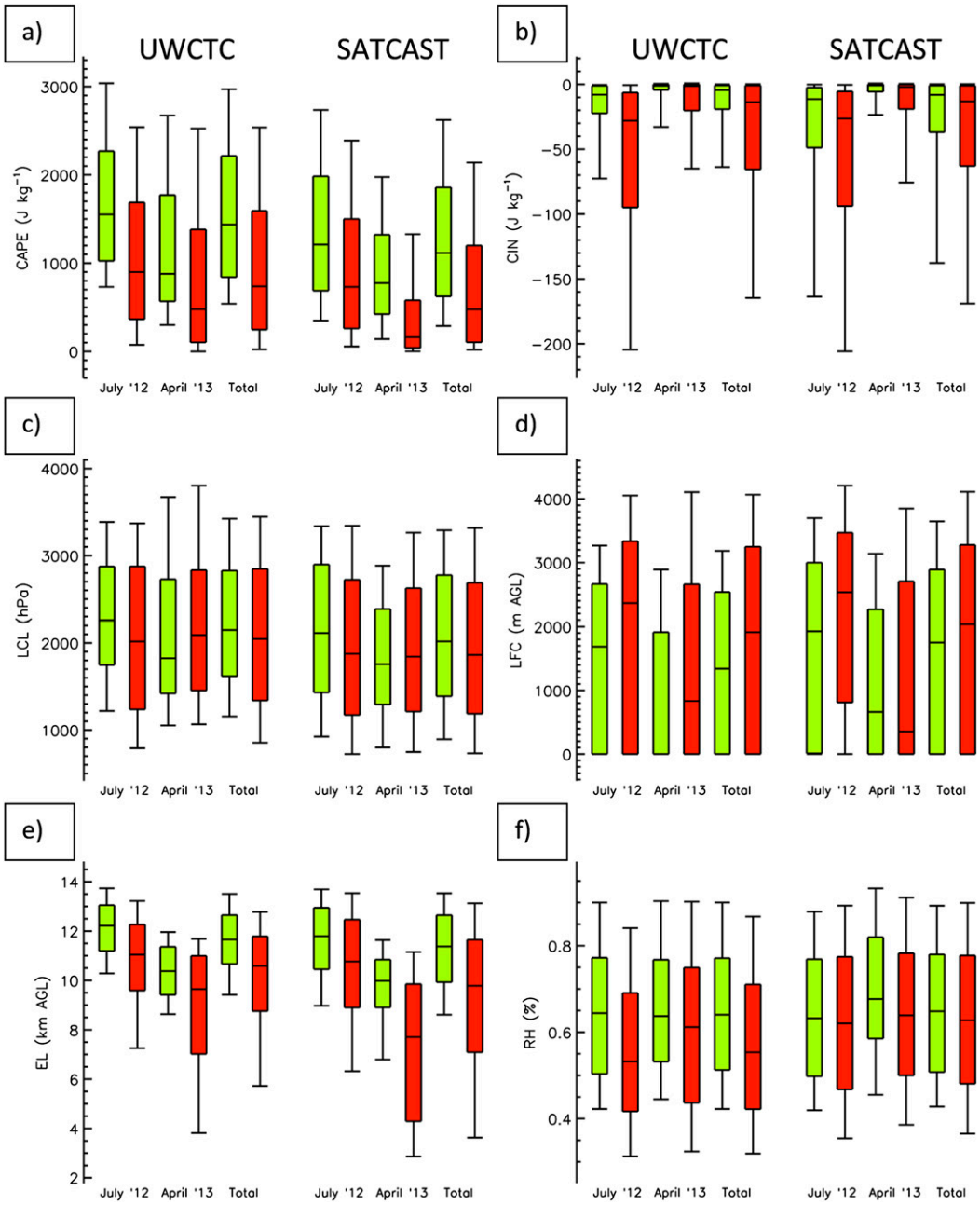

FIG. 11. July, April, and total UWCTC and SATCAST study-period RAP values for positive (green) and negative (red) indications. Boxes represent the 25th–75th percentiles, and whiskers are from the 10th to the 90th percentiles. Medians are shown as solid lines within the boxes.

indications as reasonable forecasts, similar skill scores were found for CTC indications as reported in Sieglaff et al. (2011) and Hartung et al. (2013). Upon further inspection it was found that the increased FAR (decreased POD) directly resulted from the exclusion of indications that occur on convective systems after CI was detected.

If CTC indications are considered to be positive for a 17-min period after CI detection [as in Hartung et al. (2013)], the objective validation used here produces validation statistics that are similar to those of previous studies. Allowing for successful CTC indications after CI provides no benefit to environmental analysis, however, and risks contaminating environmental-data collection with respect

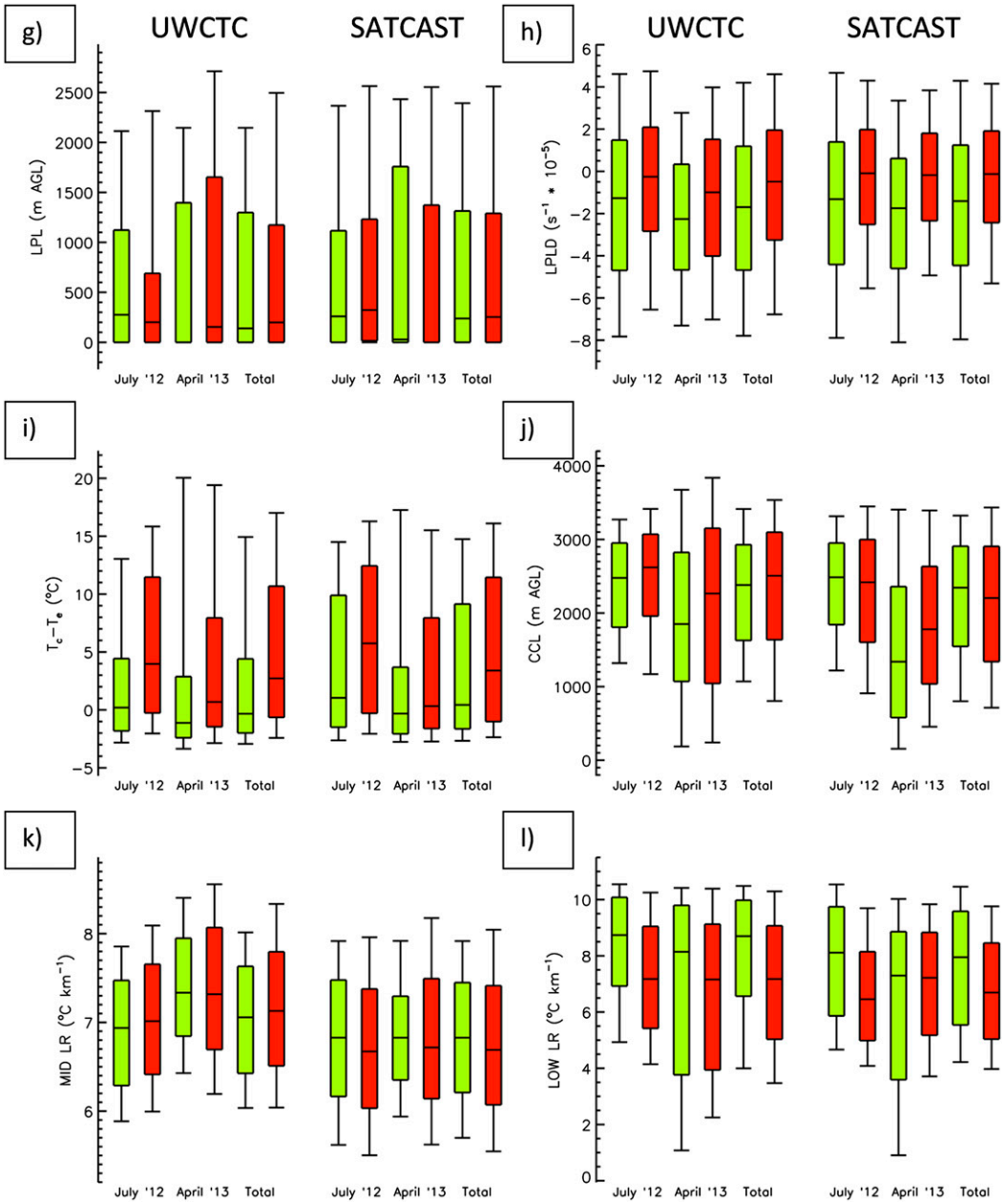

FIG. 11. (*Continued*)

to performance (Fig. 6). All positive post-CI CTC indications occur within close proximity to ongoing convection and, therefore, are excluded from an environmental analysis regardless of objective positive or false classification. Post-CI CTC false indications are not always in close proximity to ongoing convection and, therefore, could be included in an environmental analysis. It is crucial to classify post-CI CTC indications as false for a correct assessment of environmental influence on CTC algorithm performance with a model that cannot resolve convective time scales. Thus, all validations in this study are not a finalized evaluation of algorithm "skill." Rather this validation technique is good for objectively identifying regions where positive or false indications occur for environmental analysis. Therefore, validation statistics (POD, FAR, CSI, and Brier score) should not be calculated using this method. Objective validation methods for environmental analysis that do include post-CI indications will need to use models that sufficiently resolve convective-scale motions.

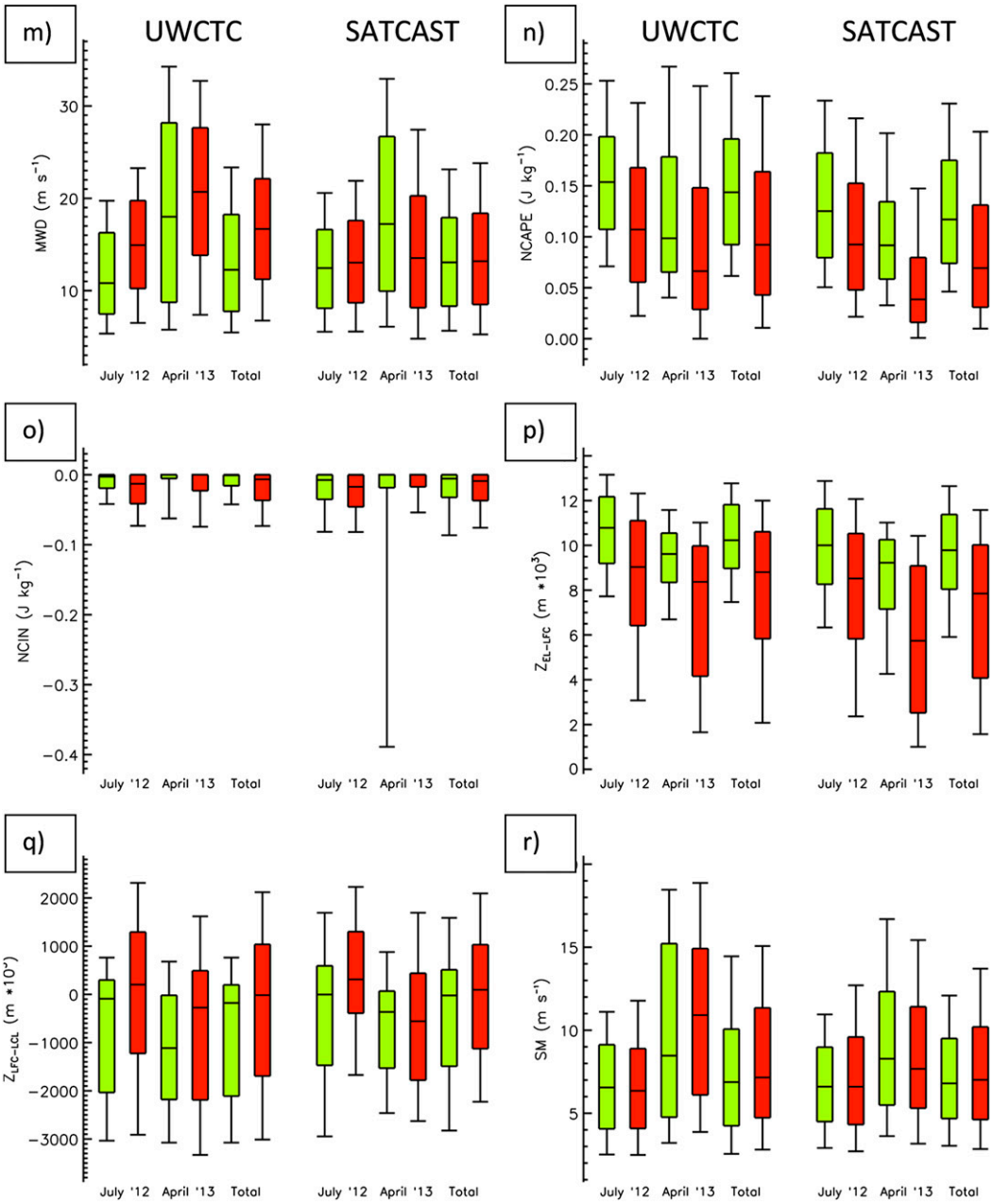

FIG. 11. (*Continued*)

a. Principal component analysis

PCA is the first step in this statistical examination. PCA for the UWCTC indications determined that the top two sources of variance in the July 2012 dataset explained 45% of overall variation (Table 4). The eigenvector for the first principal component (PC1) suggests that the first source of variation is related to LFC height. CIN also has a notable influence on the first source of variation, despite not being among the top five components. Variables related to LFC ($Z_{\text{LFC-LCL}}$ and $Z_{\text{EL-LFC}}$) had larger components in PC1, however. It is likely that changes in CIN are related to changes in $Z_{\text{LFC-LCL}}$. The second principal component (PC2) eigenvector was largely related to instability present, with large eigenvector components in CAPE, LCL, and NCAPE. The signs of PC1 and PC2 suggest that LFC height increases as PC1 increases and that instability decreases as PC2 increases. Dependency upon values of PC1 and PC2 becomes apparent when the principal

TABLE 6. The P values for MW tests between positive and false indications for the total dataset (combined July and April). Variables with 99.5% significance are shown in boldface font.

	SATCAST	UWCTC
CAPE	**0.000**	**0.000**
CIN	**0.000**	**0.000**
LCL	**0.000**	0.008
LFC	**0.000**	**0.000**
EL	**0.000**	**0.000**
RH	**0.000**	**0.000**
LPL	0.108	0.455
LPLD	**0.000**	**0.000**
$T_c - T_e$	**0.000**	**0.000**
CCL	**0.000**	0.042
MIDLR	**0.000**	0.009
LOWLR	**0.000**	**0.000**
MWD	0.057	**0.000**
NCAPE	**0.000**	**0.000**
NCIN	**0.000**	**0.000**
$Z_{\text{EL-LFC}}$	**0.000**	**0.000**
$Z_{\text{LFC-LCL}}$	**0.000**	**0.000**
SM	**0.000**	0.014

TABLE 7. The 9 Apr 2013 confusion matrices for UWCTC and SATCAST performance of QDA, removing insignificant variables as diagnosed by MW.

		UWCTC predicted		
		False	Positive	Total
UWCTC actual	False	88	34	122
	Positive	27	11	38
	Total	115	45	160
Percentage of improvement:			1.08%	
		SATCAST predicted		
		False	Positive	Total
SATCAST actual	False	9154	9546	18 700
	Positive	153	282	435
	Total	9307	9828	19 135
Percentage of improvement:			13.78%	

component scores are plotted (Fig. 7). Positive indications favor areas with lower-than-average LFC heights, with ~80% of positive indications occurring in areas with PC1 < 0. The dependence on CAPE is not as clear with the July PCA. It is notable that there are a larger number of positive indications in more-unstable regions. However, the relative difference between quadrants is too small to make a definitive conclusion about CAPE using only PCA.

The April 2013 UWCTC data PCA displays similar sources of variation as do the July data (Table 4). PC1 and PC2 again explain the majority of the variation (~52%). The April PC1 did not lend itself to the same interpretation as the July PC1, however. The April PC1 dependence did not appear to be linked with LFC height, given the relatively low magnitude of the $Z_{\text{EL-LFC}}$ eigenvector component. The April PC1 did display a dependence on $Z_{\text{LFC-LCL}}$, with another notably large magnitude on LOWLR. This lends itself to the interpretation that higher April PC1 scores suggest environments conducive to deeper stable layers that are visible by satellite. April PC2 again is related to instability, with higher PC2 scores being almost directly linked to less statically unstable environments. The differences between July and April variation suggest that the choice of initial distributions for probability-based discrimination should vary for different time periods. April UWCTC also suggests dependence on both the amount of instability and stability in the atmosphere. Almost 80% of all positive indications occur in more-unstable regions (Fig. 8). Since almost 50% of positive indications occur in areas with both larger instability and smaller $Z_{\text{LFC-LCL}}$ layers, PCA suggests that there is a relationship between instability and stability with respect to UWCTC performance.

The PCA for the July SATCAST dataset (Fig. 9) had similar variations that were explained with the top five eigenvectors (Table 5). PCA for SATCAST has a much larger sample size of points in the July dataset than for UWCTC (Figs. 6 and 7). The SATCAST July PC1 suggests similar dependence on LFC height to that seen for UWCTC. Larger PC1 scores are related to lower LFC heights, lower $Z_{\text{LFC-LCL}}$, and higher $Z_{\text{EL-LFC}}$. PC2 for the July SATCAST also displays a dependence upon instability, with a notably large component for storm motion. Thus, higher PC2 scores suggest slow-moving storms in more unstable environments. The PCA plot for July SATCAST (Fig. 9) suggests a much larger performance on PC2 than does that for the UWCTC. Positive indications are clustered in environments with lower LFCs and higher instability (with ~56% of all positive indications in the top-right quadrant of Fig. 9). Few positive indications are observed below a PC2 score of −3, suggesting that there exists a minimum necessary instability factor for a SATCAST indication to be positive.

The April SATCAST PC1 has large dependence on values related only to $Z_{\text{LFC-LCL}}$ and excluded values related to the actual value of CIN (Table 5). This result displays a consistently large source of variation explained by $Z_{\text{LFC-LCL}}$ throughout all CTC-based products. It is notable that SATCAST in April is also sensitive to LFC height. The lack of a robust $Z_{\text{EL-LFC}}$ component prevents an interpretation that is based only on LFC, however. The April SATCAST PC2 is again

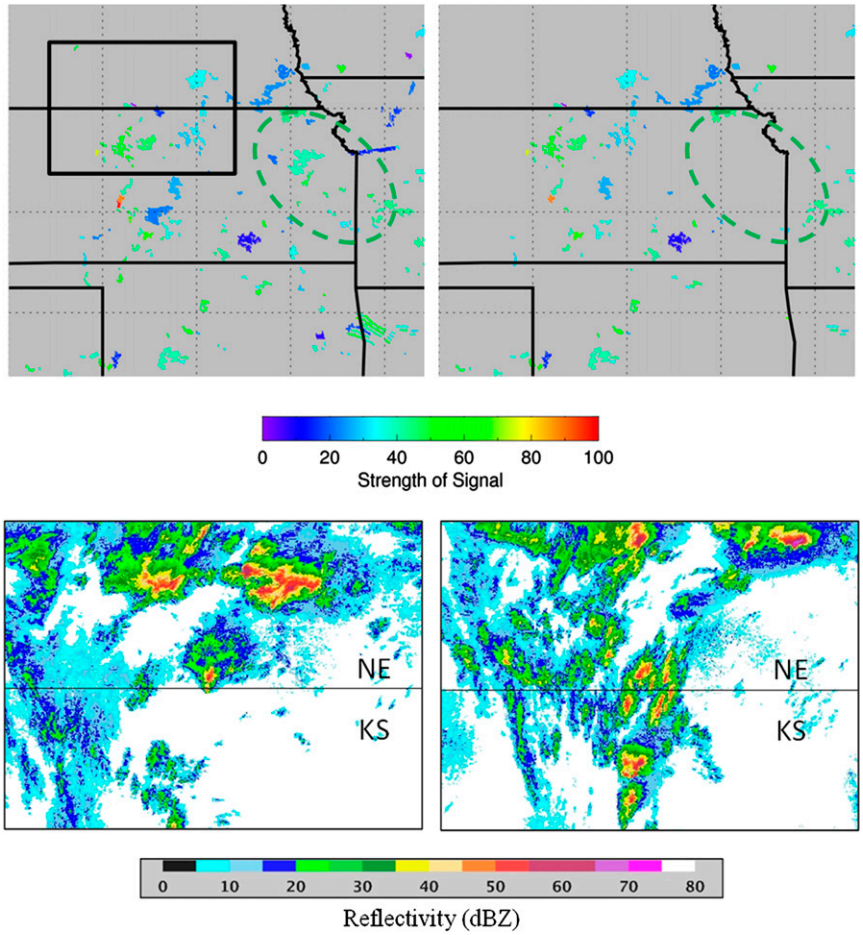

FIG. 12. The 1832 UTC 9 Apr 2013 (top left) unfiltered and (top right) QDA-filtered SATCAST. The green-dashed circle displays an area where QDA successfully removes nonconvective SATCAST indications. Also shown are the (bottom left) 1835 UTC 9 Apr 2013 composite NMQ radar reflectivity data (dBZ) inside the rectangle and (bottom right) 1935 UTC 9 Apr composite radar reflectivity (dBZ), displaying several CI events (>35 dBZ) that were successfully forecast by SATCAST.

instability, with the largest components of eigenvectors in CAPE and related variables.

Further analysis of the first two principal components of April SATCAST yields two distinct clusters of positive indications (Fig. 10). Since the first component is again related to the depth of the stable layer, the first positive detection cluster appears to occur when instability is low or nonexistent. The apparent PC1 minimum is caused by data censorship when CIN = 0; thus, the PC1 score near ~3 should be interpreted as near-zero stability with very low or negative $Z_{\text{LFC-LCL}}$. This result raises the question of why a second cluster would be seen with relatively large (in compared with the first) values of $Z_{\text{LFC-LCL}}$. The clustering could be caused by the abundance of forced convection in April, yielding two different stability environments in which convection is witnessed. Despite this clustering, again a majority of positive indications are located in areas with small $Z_{\text{LFC-LCL}}$ values and large instability.

Throughout all four PCA analyses, it becomes clear that the largest source of variation in the overall data is related to $Z_{\text{LFC-LCL}}$. This large variation does not mean that $Z_{\text{LFC-LCL}}$ is a better discrimination variable to use than CIN. Determining which variable is a better discriminator is done using MW testing. Although it is possible to create plots along the PC3, PC4, and PC5 values for all study periods, the plots for PC1 and PC2 were sufficient to conclude that a general relationship is apparent between environmental variables and CI algorithm performance. For a more detailed analysis of just what that relationship is, tests for statistically significant differences are analyzed. Finding a general

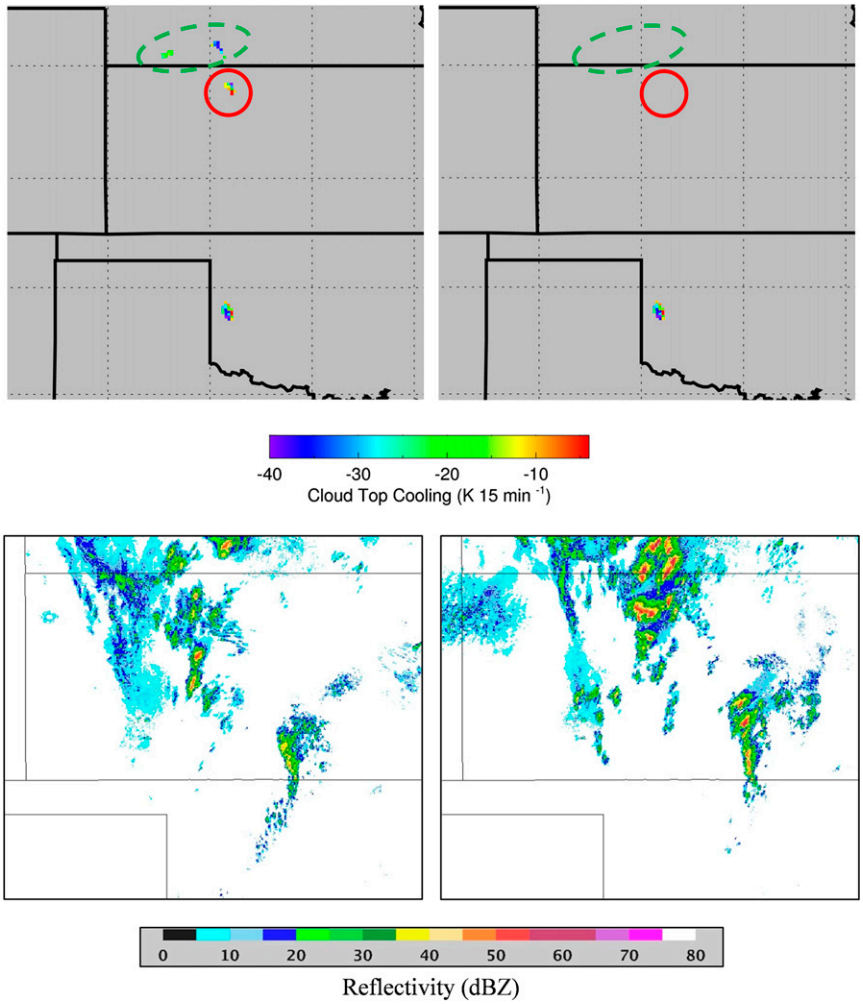

FIG. 13. The 1855 UTC 9 Apr 2013 (top left) UWCTC product with one positive detection in northern Kansas and three false detections and (top right) with a QDA filter applied to the product. Also shown are (bottom left) the 1855 UTC 9 Apr 2013 NMQ reflectivity data (dBZ) and (bottom right) the reflectivity data 1 h later. Two false detections are correctly dropped (dashed green circles in top panels) at the cost of one positive (red circles).

relationship with the largest sources of variation ($Z_{\text{LFC-LCL}}$ and CAPE) does suggest that one or the other should be important.

b. Variable contribution

Several variables appear to have statistically significant differences upon initial examination (Fig. 11). Variables such as CAPE and $Z_{\text{EL-LFC}}$ vary as expected, with notably larger values for positive indications than for false indications in UWCTC and SATCAST (Figs. 11a,p). The importance of instability is also found in LFC and EL differences where positive indications have lower LFC values and higher EL values than false indications for both algorithms (Figs. 11d,e). CIN-related variables also have a consistent relationship, such that false indications are found in more stable regions for UWCTC (Figs. 11b,o,q). Relative humidity variables are consistently different across the time periods for UWCTC, for which larger RH is seen with positive indications (Fig. 11f). Note that $T_c - T_e$ also appears to have a relationship with performance, since lower values are common with positive indications (Fig. 11i). Several preconvective environmental relationships yield differences that change depending on the time period. LPL is larger for positive UWCTC indications in July than for false indications. Positive-indication LPL is lower than for false indications for April (Fig. 11g). The same characteristic is witnessed in UWCTC LCL, MIDLR, and SM (Figs. 11c,k). The total dataset (combination of July and April study periods)

with variables that exhibit differing relationships (such as UWCTC LPL, LCL, MIDLR, and SM) ends up being relatively similar (no significant difference should be found). If no significant difference is found, then the variables are deemed not important to QDA and potentially not important to overall algorithm performance.

SATCAST RAP environmental-variable results have similar characteristics to UWCTC values (Fig. 11). Instability-related factors (e.g., CAPE, EL, and $Z_{\text{EL-LFC}}$,) all show large differences (Figs. 11a,e,p) in a manner consistent with the PCA findings (i.e., more instability and higher likelihood of a positive detection). Other variables, such as LFC, LCL, LPL, CCL, MWD, and SM, exhibit different tendencies depending on the time period (Figs. 11c,d,g,j,m,r). Variables that have differing relationships between time periods for positive and false groups result in little change when considered as a total dataset. For example, CCL is larger for positive indications than for false indications in the July study period for SATCAST (Fig. 11j). In the April study period for SATCAST, positive indications have a much lower CCL than do false indications. The resulting total dataset exhibits a difference that is not statistically significant. Other data, such as RH and SM, do not exhibit large differences between positive and false SATCAST indications for both time periods (Figs. 11f,r).

The total UWCTC dataset has several statistically significant differences between positive and false indications in MW tests (Table 6). MW suggests that MIDLR, LCL, LPL, CCL, and SM differences are not statistically significant. Fewer variables are found to not have statistically significant differences between SATCAST positive and false indications. LPL and MWD differences are not statistically significant. Statistical differences could be caused by the object-identification schemes used by each algorithm. UWCTC is a fairly conservative algorithm that only produces indications if a cloud object is deemed vertically cooling. The SATCAST identification scheme identifies all cloud objects rather than only vertically cooling areas, which produces more indications in nonconvective areas. Changing statistical differences between both algorithms for two different time periods imply that different relationships could be more important at different times of the year. Examining seasonality changes is beyond the scope of this writing, but future studies with larger datasets could explore seasonal relationships further. Now that statistically significant variables have been identified, the total study periods can be applied to future case studies with QDA.

c. *Case studies*

The QDA approach improved both UWCTC and SATCAST for the first case study (9 April 2013; Table 7).

TABLE 8. As in Table 7, but for 20 May 2013.

		UWCTC predicted		
		False	Positive	Total
UWCTC actual	False	15	79	94
	Positive	7	70	77
	Total	22	149	171
Percentage of improvement:			6.87%	
		SATCAST predicted		
		False	Positive	Total
SATCAST actual	False	9845	21 031	30 876
	Positive	302	798	1100
	Total	10 147	21 829	31 976
Percentage of improvement:			4.43%	

Important indications are kept in central Kansas, which result in CI approximately 1 h later (Fig. 12). Several false indications with relatively high SoS values are removed from areas such as eastern Kansas. The resulting POI value near 14% improves the Brier scores for the dataset. UWCTC saw a notably smaller improvement with POI near 1%. Several positive indications are lost in the 9 April 2013 case for the UWCTC dataset behind the cold front (Fig. 13). Indications are in regions containing little instability and thus are deemed environments that are not conducive to positive indications.

An examination that uses MW on the 20 May 2013 (Table 8) case study finds several false indications correctly removed from the SATCAST and UWCTC datasets (Figs. 13 and 14). Both SATCAST and UWCTC show impressive lead time in forecasting the strong updraft on the storm that produced the Moore tornado. These values are correctly kept in all analyses, and false indications are correctly removed around central Nebraska. The QDA successfully keeps what is probably the strongest of the updrafts that were analyzed in this study with the Moore cell, where cooling values of $\sim$62 K $(15\,\text{min})^{-1}$ are observed with an apparent bounded weak-echo region on the composite NMQ dataset.

A notably larger improvement in the UWCTC dataset using QDA is found in the 20–22 June 2013 case studies, for which only $\sim$19% of positive indications were considered to be false by the filtering process. The QDA removed $\sim$33% of false indications, resulting in an $\sim$14% improvement (Table 9). SATCAST displayed considerable improvement as well (Fig. 15). It is found that several false indications are left unfiltered near the area of interest, however. These indications contain relatively large SoS values and, if left unchecked, may cause confusion to a nowcaster who uses such products.

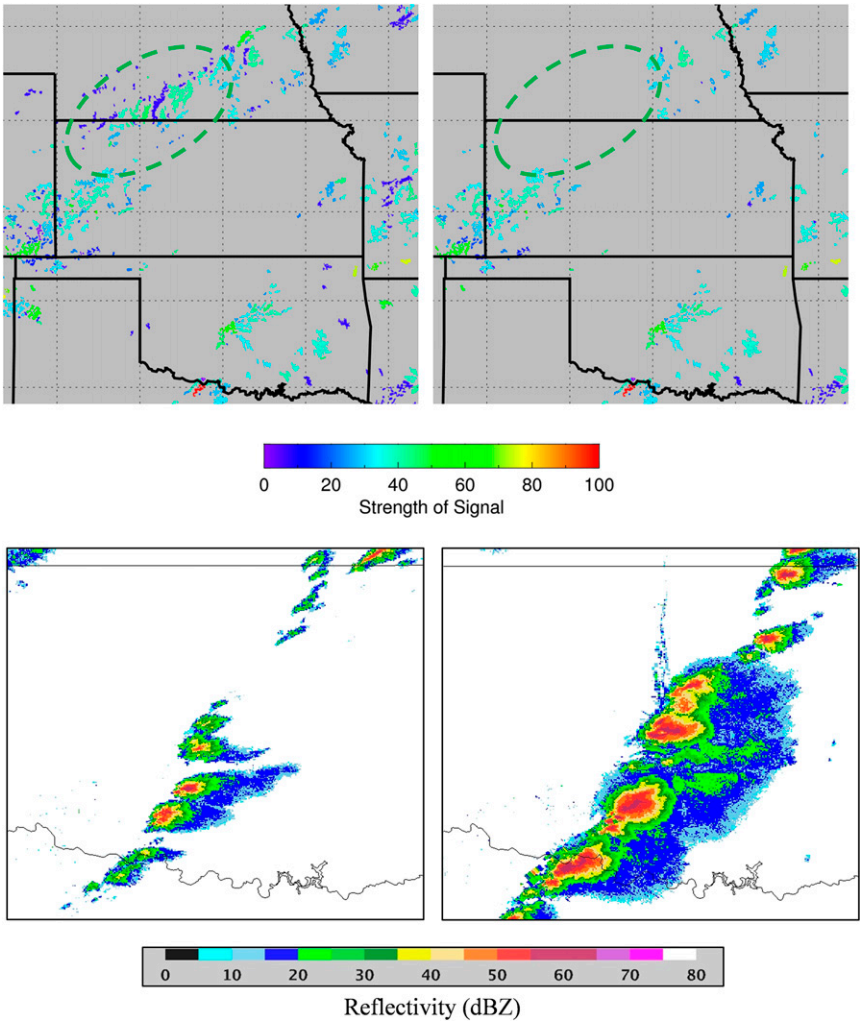

FIG. 14. The 1825 UTC 20 May 2013 (top left) unfiltered and (top right) QDA-filtered SATCAST data. The green-dashed circle highlights an area where false detections are correctly removed. Also shown are (bottom left) the 1910 UTC 20 May 2013 NMQ reflectivity data (dBZ) over central Oklahoma and (bottom right) the reflectivity data 1 h later.

Combined use of the SATCAST and UWCTC datasets in this case is found to be helpful, with both containing CI indications in northern Nebraska, resulting in several CI events (Figs. 16 and 17). The lack of filtering on several large SATCAST indications suggests that, while a QDA does arguably improve the satellite-based CTC forecasting dataset, the filtering method does not remove all false indications. A forecaster therefore should still couple this product with several other observational tools (surface data, soundings, and high-resolution models) to correctly nowcast CI in specific areas. A QDA-filtered dataset should therefore be considered only for decision support.

The 25 June 2013 case showed some of the largest percentage improvements for both UWCTC and SATCAST (Table 10). Several false indications are correctly removed from SATCAST, which correctly detects the small nocturnal line of CI in central Nebraska (Fig. 18). Although UWCTC did not pick up this line, indications for several additional events are found in central Iowa (Fig. 19). QDA successfully filters two separate indications, keeping a positive yet relatively weak [$\sim$7 K (15 min)$^{-1}$] CI indication in central Iowa and discarding a moderate [$\sim$14 K (15 min)$^{-1}$] yet false indication in central Missouri.

Overall, simple application of QDA is found to improve all case studies examined herein. Although it does not remove all false indications from the two algorithms, it does show that it is possible to successfully apply NWP variables to a CTC-based algorithm to improve the skill

TABLE 9. As in Table 7, but for 20–22 Jun 2013.

		UWCTC predicted		
		False	Positive	Total
UWCTC actual	False	133	272	405
	Positive	23	102	125
	Total	156	374	530
Percentage of improvement:			14.44%	
		SATCAST predicted		
		False	Positive	Total
SATCAST actual	False	18 845	35 474	54 319
	Positive	74	379	453
	Total	18 919	35 853	54 772
Percentage of improvement:			18.36%	

of the overall product. Therefore, probability-based filters should be used with unfiltered products and other datasets to improve the situational awareness of a CI nowcaster.

4. Summary and conclusions

Convection initiation can be determined using satellite-based brightness-temperature and interest-field trends. UWCTC and SATCAST algorithms both make use of differing CI forecasting techniques that will utilize the Advanced Baseline Imager on board the GOES-R series. Both algorithms are being extensively tested before they become operational after the launch. While several studies have examined algorithm performance and relation to severe-weather occurrence, only a few have speculated on the influences of unfavorable preconvective environments. This study therefore set out to answer three questions: Do preconvective environments have an impact on satellite-based CI forecasting algorithms? Can preconvective environmental variables be applied to new satellite products through a data-fusion process? Is forecast skill improved through the incorporation of preconvective environmental variables into the CTC algorithms? To answer all three questions, an objective validation study was conducted to create a large dataset of positive and false indications for both algorithms. Positive and false indications were examined with Rapid Refresh–resolved preconvective environmental variables using a principal component analysis, and significant differences between both groups were determined. Environmental variables that were significantly different between groups were used to filter five case studies using a quadratic discriminant analysis approach.

Objective validation took place in several steps. NMQ radar data are segmented using the WDSS-II framework, and the centroids of the segmented clusters are tracked through space and time using ThOR. Tracking allows for the identification of the first occurrence of a segmented WDSS-II cluster, also known as the point of convection initiation. The WDSS-II settings that best matched the clusters as identified by a forecaster are used.

The objective validation results in large positive and false samples of SATCAST and UWCTC indications. Study periods are taken from the late convective season in 2012 and early convective season in 2013 over the Great Plains. Study periods depended upon data availability from GOES, NMQ, and RAP data sources. A principal component analysis was completed on the

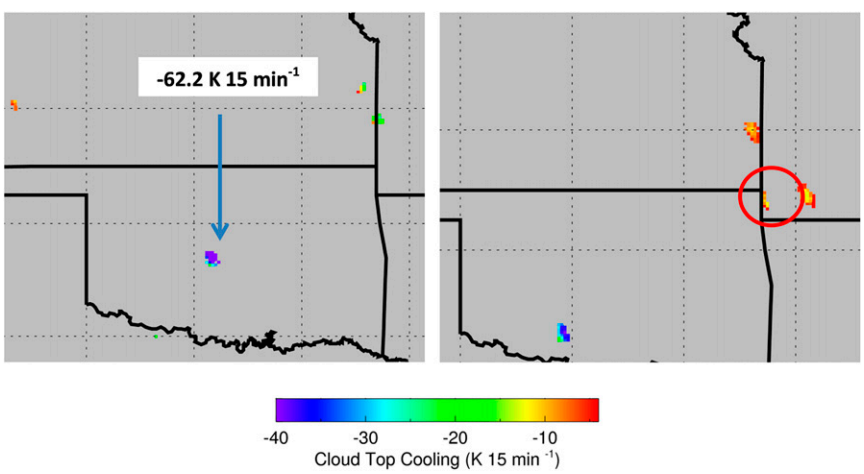

FIG. 15. (left) The 1910 UTC 20 May 2013 UWCTC product with QDA filtering and the maximum value of measured cooling for the Moore tornadic supercell, and (right) an 1815 UTC 20 May 2013 example of correctly QDA-filtered UWCTC product (circled in red).

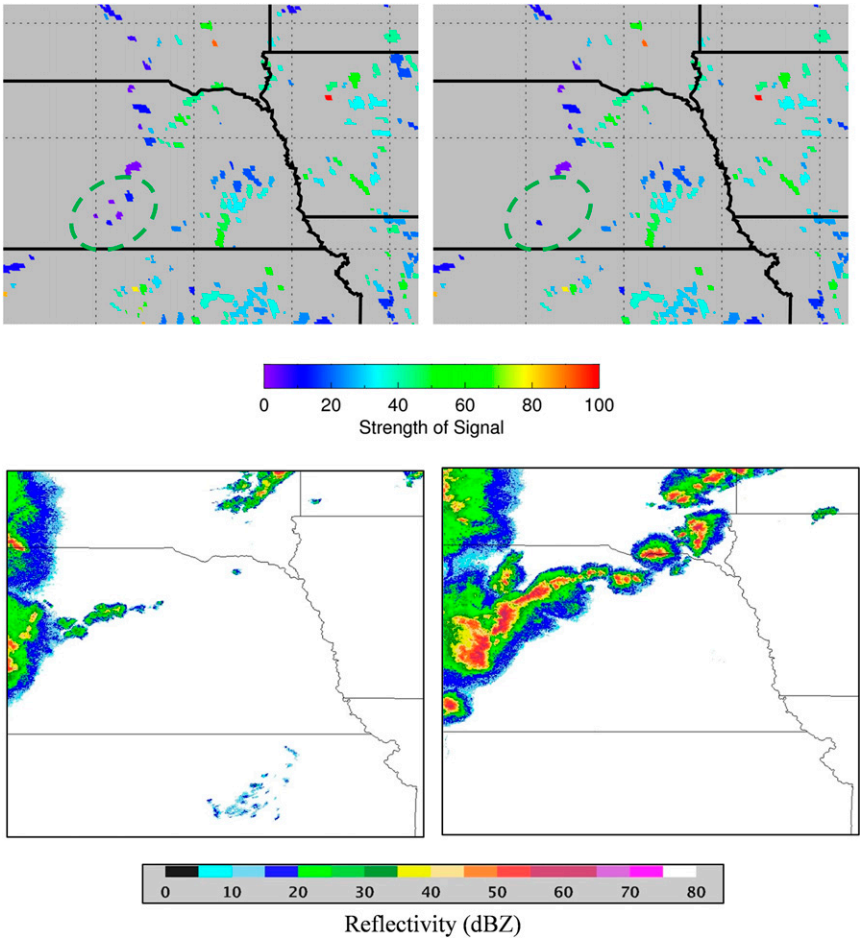

FIG. 16. The 0055 UTC 22 Jun 2013 (top left) unfiltered and (top right) QDA-filtered SATCAST data. The green-dashed circle highlights an area where false detections are correctly removed. Also shown are (bottom left) the 0125 UTC 22 Jun 2013 NMQ reflectivity data (dBZ) over central Nebraska and (bottom right) the reflectivity data 1 h later.

data to examine the sources of variation in the entire dataset. An examination of data plotted in terms of the top two sources of variation (related to $Z_{\text{LFC-LCL}}$ and CAPE) suggests that a relationship exists between how good an indication-forecast of convection initiation is and the preconvective environment. PCA found that more positive indications exist in environments that are conducive to larger-than-average CAPE and lower-than-average CIN.

Significance testing was also performed to further the exploration of relationships between preconvective environments and the satellite-algorithm performances. Larger (smaller) CAPE is found with indications that are positive (false) CI forecasts. The relationship with CAPE is possibly due to the difficulty of identifying areas that are actually undergoing vertical cooling rather than falsely resolved horizontal changes. CAPE is found in truly convective areas, where false areas (identified as objects in SATCAST or vertically cooling pixels in UWCTC) can reside in both unstable and stable regions.

In addition to CAPE, CIN is an important variable to consider for algorithm performance, which is consistent with speculations from Mecikalski et al. (2008) and Walker et al. (2012). Low-level divergence is also a helpful discrimination variable when resolved at the LPL through RAP data. Therefore, it is apparent that preconvective environments do affect the performance of satellite-based CI forecasting algorithms. No definitive conclusion can be reached with regard to the impact of shear, lapse rates, convective condensation level, layer relative humidity, and lifted condensation level because of the varying relationships between time periods. It is possible that all four variables have little impact on the overall performance of either algorithm. Storm motion is not significant for the likelihood of a positive or false indication. The storm-motion problem

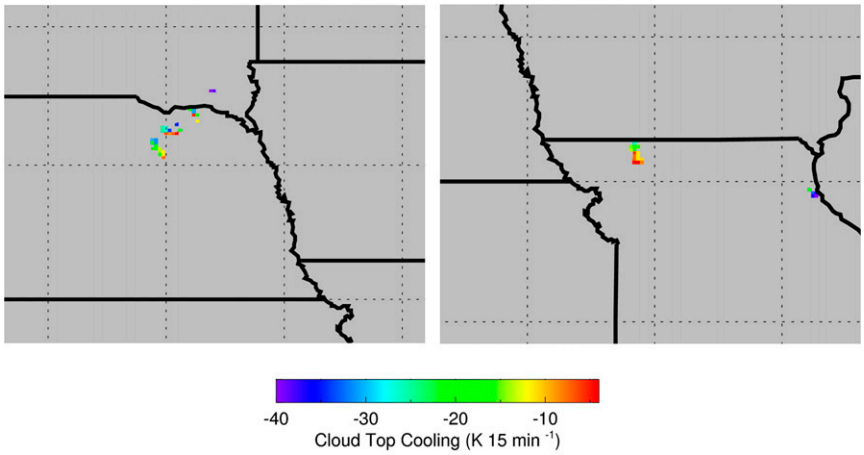

FIG. 17. (left) The 0125 UTC 22 Jun 2013 QDA-filtered UWCTC product over northern Nebraska, and (right) a 0155 UTC 22 Jun 2013 example of two correctly removed products in the nonconvective area of northern Missouri.

may stem from an issue about missed detections rather than likelihood of an indication performing well. Any issues regarding storm motion are heavily dependent upon the temporal resolution of the satellite imagery and should be examined in further detail after the launch of the GOES-R series.

All significant variables, including CAPE, CIN, divergence, and related variables, are then used in a probability-based QDA. Use of the QDA consistently improved the performance of both algorithms when the proper variables were removed from the analysis. Even though MW does not remove some of the inconsistent variables discussed previously, the overall algorithm is still improved with application of the QDA. Thus, it is shown that differences exist in the preconvective environments for positive and false indications in both algorithms. The application of the statistically significant environmental variables resulted in improvement in both products. Data fusion did not remove several important indications, including the Moore cell. The successfully developed QDA filtering process showed that it is possible to statistically combine NWP variables with satellite-based CI forecasts, and the new data-fused product can reduce indication noise and improve the skill of the forecasts.

Comparison of radar data with CTC indications can introduce issues stemming from unresolved parallax problems. Spatial decorrelation between radar and satellite data is also possible because the two datasets are measuring two different things: radar measures the droplet distribution in an area, and CTC or cloud-based interest fields measure the area of a cold cloud-top temperature. Both issues are accounted for in this study, but a better validation in future data periods can take advantage of the GOES-R Geostationary Lightning Mapper (GLM; http://www.goes-r.gov) to determine locations of convection initiation. The GLM will not suffer from issues stemming from parallax, beam blockage, or lack of radar coverage, and much larger domains can be used for validation.

Sieglaff et al. (2013) also suggest that a validation that is based on the tracking and identification of cloud objects may be a better approach to identifying convective events than a radar-based event-identification method. The advantage of cloud-object identification stems from the ability to diagnose correct null forecasts, in which a cumulus pixel exists without a CTC indication. The diagnosis of correct null forecasts will allow for the computation of Heidke skill scores. The reason that a cloud-object approach was not adopted for this work was that the current generation of GOES has very low temporal resolution (normally 7–15 min, with 30-min data gaps every 3 h for full disc scans). The cloud-object approach could result in a better objective validation

TABLE 10. As in Table 7, but for 25 Jun 2013.

		UWCTC predicted		
		False	Positive	Total
UWCTC actual	False	54	28	82
	Positive	3	7	10
	Total	57	35	92
Percentage of improvement:			35.85%	
		SATCAST predicted		
		False	Positive	Total
SATCAST actual	False	10 352	9239	19 591
	Positive	28	100	128
	Total	10 380	9339	19 719
Percentage of improvement:			30.96%	

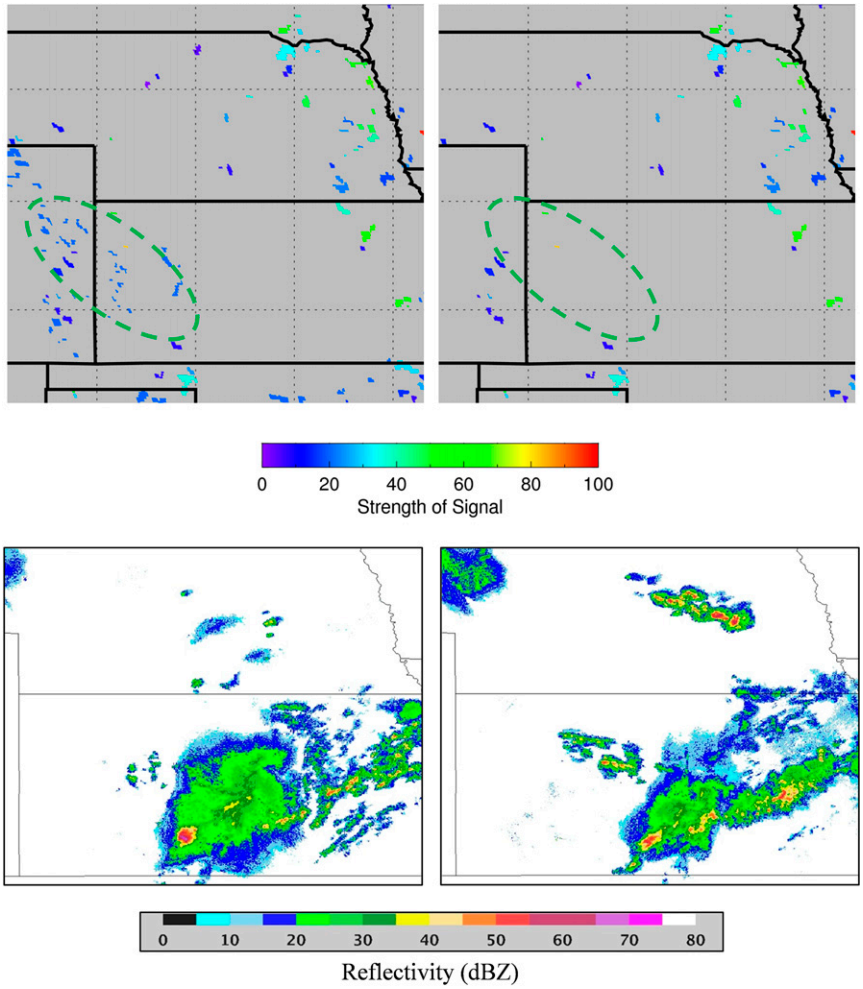

FIG. 18. The 0215 UTC 25 Jun 2013 (top left) unfiltered and (top right) QDA-filtered SATCAST data. The green-dashed circle highlights an area where false detections are correctly removed. Also shown are (bottom left) the 0215 UTC 22 Jun 2013 NMQ reflectivity data (dBZ) over southern Nebraska and (bottom right) the reflectivity data 1 h later.

after the launch of GOES-R because temporal resolution will increase to 5 min.

Several problems occur when tracking large-volume datasets such as SATCAST. The ThOR method, to consider all tracks in an acceptable range, had to be tweaked to handle the low temporal resolution of GOES and the high object density of SATCAST. Without correction, ThOR would consider too many candidate tracks with SATCAST objects for reasonable computation. The reduction in first-guess search radius allowed ThOR to produce usable tracks with reasonable computational time. Some tracking error is expected with the reduction in search radius, particularly with fast-moving cloud objects that could be lost by ThOR's tracking scheme. Future studies with an ~5-min GOES-R temporal resolution should not have the same tracking issues.

An issue that may have occurred in the QDA is that convective contamination is not considered in the application of RAP-based variables to new cases. Ongoing convection processes contaminating RAP analysis were not included in new cases so as to simulate the performance of QDA under real-time conditions. With this approach, all products are filtered with the approximate environment in which they are situated. This limitation of RAP data (temporal granularity) may explain some of the performance variability of the QDA filter on differing case studies. As higher-temporal-resolution models become operational, such as the higher-temporal-resolution Rapid Refresh, QDA-filtered data performance should improve in the real-time environment. Another issue that may have occurred in QDA is the fact that SATCAST SoS values take into account convection-related variables that were not removed by

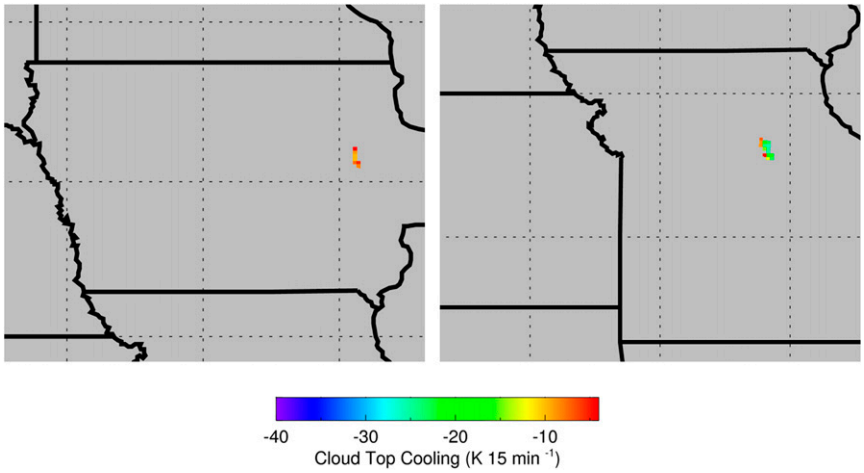

FIG. 19. (left) The 0815 UTC 25 Jun 2013 QDA-filtered UWCTC product over Iowa, and (right) a 0945 UTC 25 June 2013 example of a UWCTC removed value.

this analysis. Removing variables that are not statistically different from the QDA increased the observed percentage of improvement. Variables that are not statistically different that are used in the calculation of SoS can mitigate the improvement of QDA. Future products can take into account the observed statistical relationships in this work to improve output when fusing indications with NWP data. Also, all derived relationships are found on the current GOES-series Proving Ground products, which have a lower temporal resolution than is projected for GOES-R. It was not the goal of this study to make the perfect QDA, however. The goal of this study was to show that it is possible to apply specific environmental variables to improve current products, and this goal was successfully achieved. This study has thus created the initial framework for future examinations of preconvective environmental influence on CTC and interest-field forecasting. New, more-skillful data-fused products should improve the situational awareness of CI nowcasters.

Acknowledgments. We thank Dr. Adam Houston and Dr. Matthew Van Den Broeke for the advice they have provided for this project. This project was also greatly aided by cooperation from multiple institutions. We are grateful to Dr. John Mecikalski, John Walker, and Chris Jewett from the University of Alabama in Huntsville and to Justin Sieglaff and Wayne Feltz from the University of Wisconsin–Madison. This project also benefited from the direction and feedback that were provided by forecasters at the National Weather Service in Omaha/Valley, Nebraska. This project was completed with the help of several meteorology students, including Adam Taylor, Casey Griffin, Nathan Jurgensen, and Katie Rourke. This project also benefited from help provided by Noah Lock, who assisted with objective segmentation and tracking for radar and satellite data. We are also thankful to the University of Nebraska—Lincoln Earth and Atmospheric Sciences Department, who provided the facilities and computational power that made this project possible. This project was funded in part by a subaward with UCAR under the sponsorship of NOAA/DOC as part of the COMET Cooperative project Z11-91842.

APPENDIX

Subjective Validation Technique

A small dataset of radar-observed deep convection from 25 July 2012 (Fig. 1c) is examined to determine which WDSS-II settings would work best for an objective scheme. The domain that is used is from 2000 UTC 25 July to 0000 UTC 26 July 2012 because of the abundance of CI events. The validation process begins with forecasters at the University of Nebraska identifying events they believed to be CI in this time frame, which are referred to as ''truth'' clusters. Forecasters identified

TABLE A1. The minimum scales with the highest skill values shown for validation of w2segmotionll–ThOR CI clusters in comparison with subjectively identified truth CI clusters. The w2segmotionll settings are presented as low smooth (50th-percentile smoothing over a 5 × 5 box), medium smooth (50th-percentile smoothing over a 7 × 7 box), and high smooth (50th-percentile smoothing over a 9 × 9 box).

Half-size in pixels (smoothing)	Min scale in pixels (saliency)	POD	FAR	CSI
4 (high)	20	73.1	20.4	63.5
3 (medium)	30	69.7	18.6	66.67
2 (low)	40	62.7	18.6	61.2

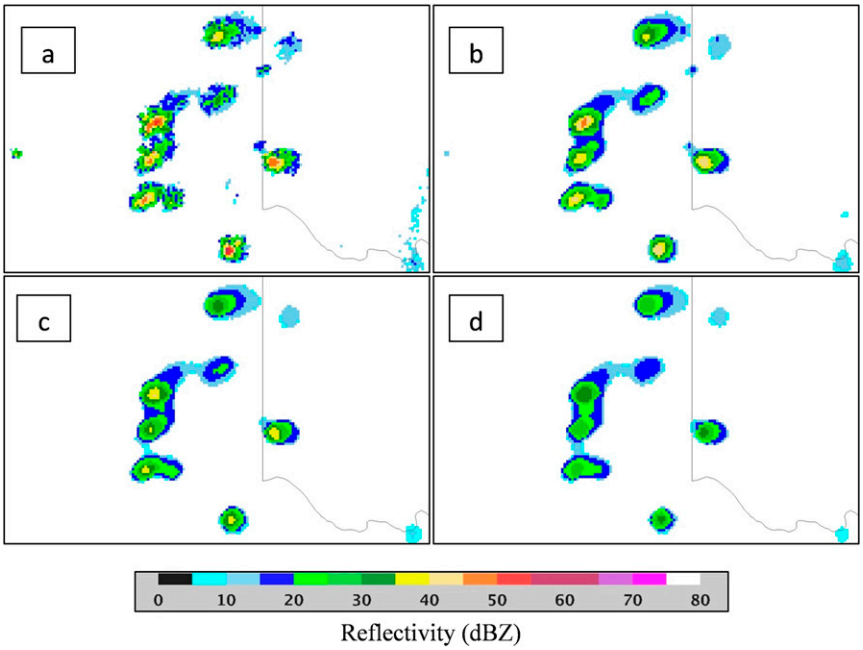

FIG. A1. (a) Example of unsmoothed composite NMQ data over the Texas Panhandle and southwestern Oklahoma. Also shown are the data with (b) light smoothing applied, with a 50th-percentile filter over a 5 × 5 box; (c) medium smoothing applied, with a 50th-percentile filter over a 7 × 7 box; and (d) heavy smoothing applied, with a 50th-percentile filter over a 9 × 9 box. Colors that are "hotter" than yellow are above 35 dBZ and are considered to be convective.

truth clusters using a spatial scale that they believed accurately represented the initial areal extent of a deep-convection event. The objective clusters are then validated with the given truth clusters.

The first variable tested is the smoothing filter that w2segmotionll uses to remove spurious peaks and noise. The default w2segmotionll setting uses a 50th-percentile filter with a box half-size of 5 (an 11 × 11 pixel box). Larger half-sizes can remove information that may be important to identifying CI events. Lowering half-sizes comes with the consequence of increased spurious peaks and noise values, and therefore half-sizes of 2, 3, 4, and 5 are tested. A minimum scale is also tested with different half-sizes. Minimum-scale saliency values of 20, 30, and 40 pixels are examined with all four half-sizes.

Four different half-sizes with three different scales are input into ThOR to determine the location of a CI event, which is then compared with the truth dataset. A ThOR CI cluster with (without) a corresponding subjectively identified truth cluster within 10 min is considered to be a positive (false) indication. A truth cluster without a corresponding ThOR cluster is considered to be a missed detection. The probability of detection (POD), false-alarm ratio (FAR), and critical success index (CSI) are determined for the w2segmotionll–ThOR objective-validation techniques as follows:

$$\mathrm{POD} = \frac{a}{a+b},$$

$$\mathrm{FAR} = \frac{c}{c+d}, \quad \text{and}$$

$$\mathrm{CSI} = \frac{d}{d+b+c},$$

where a is the number of detected CI truth clusters, b is the number of missed CI truth clusters, c is the number of false w2segmotionll–ThOR CI detections, and d is the number of positive WDSS-II–ThOR CI detections. Optimizing w2segmotionll settings will allow for robust identification of CI events that are used in objective validation.

An objective validation is designed to mimic the interpretation of CI by a forecaster. Thus, the design of the objective scheme is optimized through comparison with a subjective validation. The objective scheme that best resembles the small-scale subjective validation is used. The subjective validation revealed optimal settings for the w2segmotionll (Table A1). The default smoothing parameter (half-size of 5) is too aggressive and removed results that could be important in an objective-validation scheme. As lower and more skillful half-sizes are used, several important features became visible to the clustering process (Fig. A1). It is clear that increasing the half-sizes of the smoothing parameters allows for smaller saliency

scales to be more skillful. Less smoothing results in too many clusters being identified and thus presents a need for larger saliency scales to improve the skill scores. For this study, the medium (and most skillful) value of half-size of 3 with a 30-pixel saliency scale was chosen.

REFERENCES

Banacos, P., and D. Schultz, 2005: The use of moisture flux convergence in forecasting convection initiation: Historical and operational perspectives. *Wea. Forecasting,* **20,** 351–366, doi:10.1175/WAF858.1.

Bedka, K., and J. R. Mecikalski, 2005: Application of satellite-derived atmospheric motion vectors for estimating mesoscale flows. *J. Appl. Meteor.,* **44,** 1761–1772, doi:10.1175/JAM2264.1.

Cintineo, J. L., M. J. Pavolonis, J. M. Sieglaff, and D. T. Lindsey, 2014: An empirical model for assessing the severe weather potential of developing convection. *Wea. Forecasting,* **29,** 639–653, doi:10.1175/WAF-D-13-00113.1.

Fisher, R. A., 1936: The use of multiple measurements in taxonomic problems. *Ann. Eugen.,* **7,** 179–188, doi:10.1111/j.1469-1809.1936.tb02137.x.

Hartung, D. C., J. M. Sieglaff, L. M. Cronce, and W. F. Feltz, 2013: An intercomparison of UW cloud-top cooling rates with WSR-88D radar data. *Wea. Forecasting,* **28,** 463–480, doi:10.1175/WAF-D-12-00021.1.

Hotelling, H., 1933: Analysis of a complex of statistical variables into principal components. *J. Educ. Pscychol.,* **24,** 417–441, 498–520, doi:10.1037/h0071325.

Houston, A. L., N. A. Lock, J. Lahowetz, B. L. Barjenbruch, G. Limpert, and C. Oppermann, 2015: Thunderstorm observation by radar (ThOR): An algorithm to develop a climatology of thunderstorms. *J. Atmos. Oceanic Technol.,* **32,** 961–981, doi:10.1175/JTECH-D-14-00118.1.

Johnson, R. A., and D. W. Wichern, 2007: Discrimination and classification. *Applied Multivariate Statistical Analysis,* P. Recter et al., Eds., Pearson Education, 575–670.

Lakshmanan, V., and T. Smith, 2009: Data mining storm attributes from spatial grids. *J. Atmos. Oceanic Technol.,* **26,** 2353–2365, doi:10.1175/2009JTECHA1257.1.

——, R. Rabin, and V. DeBrunner, 2003: Multiscale storm identification and forecast. *Atmos. Res.,* **67–68,** 367–380, doi:10.1016/S0169-8095(03)00068-1.

——, T. Smith, G. J. Stumpf, and K. Hondl, 2007: The Warning Decision Support System–Integrated Information. *Wea. Forecasting,* **22,** 596–612, doi:10.1175/WAF1009.1.

——, K. Hondl, and R. Rabin, 2009: An efficient, general-purpose technique to identify storm cells in geospatial images. *J. Atmos. Oceanic Technol.,* **26,** 523–537, doi:10.1175/2008JTECHA1153.1.

Lock, N. A., and A. L. Houston, 2014: Empirical examination of the factors regulating thunderstorm initiation. *Mon. Wea. Rev.,* **142,** 240–258, doi:10.1175/MWR-D-13-00082.1.

Mann, H. B., and D. R. Whitney, 1947: On a test of whether one of two random variables is stochastically larger than the other. *Ann. Math. Stat.,* **18,** 50–60, doi:10.1214/aoms/1177730491.

Mecikalski, J. R., and K. M. Bedka, 2006: Forecasting convective initiation by monitoring the evolution of moving cumulus in daytime GOES imagery. *Mon. Wea. Rev.,* **134,** 49–78, doi:10.1175/MWR3062.1.

——, ——, S. J. Paech, and L. A. Litten, 2008: A statistical evaluation of GOES cloud-top properties for nowcasting convective initiation. *Mon. Wea. Rev.,* **136,** 4899–4914, doi:10.1175/2008MWR2352.1.

——, X. Li, L. D. Carey, E. W. McCaul Jr., and T. A. Coleman, 2013: Regional comparison of GOES cloud-top properties and radar characteristics in advance of first-flash lightning initiation. *Mon. Wea. Rev.,* **141,** 55–74, doi:10.1175/MWR-D-12-00120.1.

——, J. K. Williams, C. P. Jewett, D. Ahijevych, A. LeRoy, and J. Walker, 2015: Probabilistic 0–1-h convective initiation nowcasts that combine geostationary satellite observations with numerical weather prediction model data. *J. Appl. Meteor. Climatol.,* **54,** 1039–1059, doi:10.1175/JAMC-D-14-0129.1.

NCDC, 2013: Rapid Refresh. National Climatic Data Center, accessed 10 July 2012–July 2013. [Available online at http://nomads.ncdc.noaa.gov/data.php.]

NSSL, 2013: National Mosaic and Multi-Sensor Quantitative Precipitation Estimation (NWQ) system. National Severe Storms Laboratory, accessed 10 July 2012–July 2013. [Available online at http://nmq.ou.edu/legacy/legacy2012.html.]

Roberts, R. D., and S. Rutledge, 2003: Nowcasting storm initiation using *GOES-8* and WSR-88D data. *Wea. Forecasting,* **18,** 562–584, doi:10.1175/1520-0434(2003)018<0562:NSIAGU>2.0.CO;2.

Sieglaff, J. M., L. M. Cronce, and W. F. Feltz, 2011: Nowcasting convective storm initiation using satellite-based box-averaged cloud-top cooling and cloud-type trends. *J. Appl. Meteor. Climatol.,* **50,** 110–126, doi:10.1175/2010JAMC2496.1.

——, D. C. Hartung, W. F. Feltz, L. M. Cronce, and V. Lakshmanan, 2013: A satellite-based convective cloud object tracking and multipurpose data fusion tool with application to developing convection. *J. Atmos. Oceanic Technol.,* **30,** 510–525, doi:10.1175/JTECH-D-12-00114.1.

SSEC, 2013: University of Wisconsin cloud top cooling algorithm. Space Science and Engineering Center, accessed 10 July 2012–July 2013. [Available online at http://cimss.ssec.wisc.edu/snaap/convinit/quicklooks.]

UAH, 2013: Satellite convection analysis and tracking. University of Alabama in Huntsville, accessed 10 July 2012–July 2013. [Available online at www.nsstc.uah.edu.]

Walker, J. R., W. M. MacKenzie Jr., J. R. Mecikalski, and C. P. Jewett, 2012: An enhanced geostationary satellite–based convective initiation algorithm for 0–2-h nowcasting with object tracking. *J. Appl. Meteor. Climatol.,* **51,** 1931–1949, doi:10.1175/JAMC-D-11-0246.1.

Weisman, M. L., and J. B. Klemp, 1984: The structure and classification of numerically simulated convective storms in directionally varying wind shears. *Mon. Wea. Rev.,* **112,** 2479–2498, doi:10.1175/1520-0493(1984)112<2479:TSACON>2.0.CO;2.

Wilks, D. S., 2011: The multivariate normal (MVN) distribution. *Statistical Methods in Atmospheric Sciences,* 3rd ed., D. S. Wilks, Ed., International Geophysics Series, Vol. 100, Elsevier, 491–518.

Williams, E., and N. Renno, 1993: An analysis of the conditional instability of the tropical atmosphere. *Mon. Wea. Rev.,* **121,** 21–36, doi:10.1175/1520-0493(1993)121<0021:AAOTCI>2.0.CO;2.

Zhang, J., and Y. Qi, 2010: A real-time algorithm for the correction of brightband effects in radar-derived QPE. *J. Hydrometeor.,* **11,** 1157–1171, doi:10.1175/2010JHM1201.1.

——, and Coauthors, 2011: National Mosaic and Multi-Sensor QPE (NMQ) system: Description, results, and future plans. *Bull. Amer. Meteor. Soc.,* **92,** 1321–1338, doi:10.1175/2011BAMS-D-11-00047.1.